Research Square

Preprints are preliminary reports that have not undergone peer review.
They should not be considered conclusive, used to inform clinical practice,
or referenced by the media as validated information.

Molecular Epidemiology and Resistance Profiling of Macrolide-Resistant Bacterial Pathogens in Egyptian Primary Healthcare Centers Using Third-Generation High-Throughput Sequencing

Mohammed Kassab[1]

mohammed.kassab@pharma.cu.edu.eg

Cairo University

Research Article

Keywords: Antimicrobial Resistance, Macrolides, Egypt, Primary Healthcare, Third-Generation Sequencing, Oxford Nanopore Technologies, Pacific Biosciences, Molecular Epidemiology, Horizontal Gene Transfer, ermB, ermC, Heteroresistance, 23S rRNA Mutation

Posted Date: November 9th, 2026

DOI: https://doi.org/10.21203/rs.3.rs-11222930/v1

License: This work is licensed under a Creative Commons Attribution 4.0 International License.
Read Full License

Additional Declarations: No competing interests reported.

Molecular Epidemiology and Resistance Profiling of Macrolide-Resistant Bacterial Pathogens in Egyptian Primary Healthcare Centers Using Third-Generation High-Throughput Sequencing

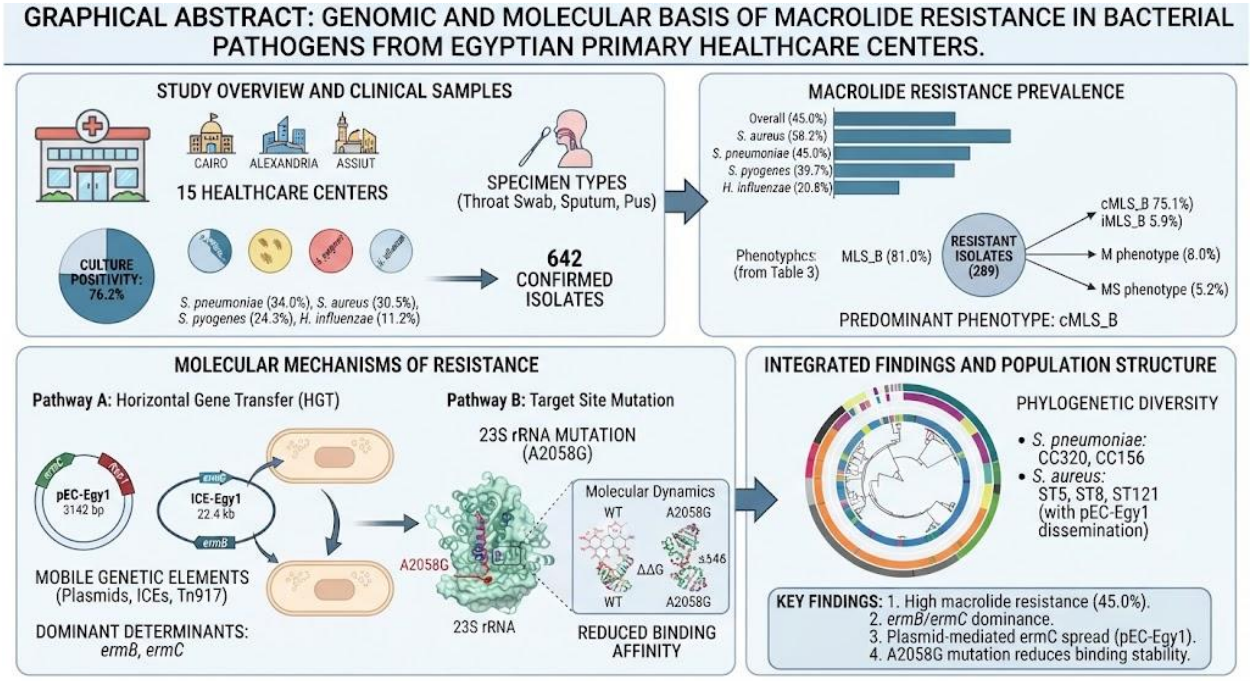
Running Title: Macrolide Resistance Genomics in Egyptian Primary Care

Article Type: Research

Author: Mohammed Kassab[1]*
Affiliation: [1]Department of Microbiology and Immunology, Faculty of Pharmacy, Cairo University, Cairo, Egypt
ORCID: 0000-0003-2554-0663
Corresponding Author: Prof. Dr. Mohammed Kassab, Department of Microbiology and Immunology, Faculty of Pharmacy, Cairo University, Cairo, Egypt
Email: mohammed.kassab@pharma.cu.edu.eg | ORCID: 0000-0003-2554-0663

Highlights

- **High Prevalence of Resistance:** Phenotypic macrolide resistance reached 45.0% among bacterial pathogens surveyed across 15 primary healthcare centers in Egypt.
- **Dominant Resistance Determinants:** ermB and ermC genes predominated significantly among resistant S. pneumoniae, S. pyogenes, and S. aureus clinical isolates.
- **Advanced Genomic Resolution:** Long-read ONT and PacBio HiFi sequencing successfully resolved complex resistance genes, plasmids, integrative and conjugative elements (ICEs), and clonal lineages.
- **Mutation & Heteroresistance Tracking:** The A2058G 23S rRNA mutation was identified in 7.6% of resistant isolates, successfully tracking complex heteroresistant bacterial subpopulations.
- **Genotype-Phenotype Linkage:** Molecular dynamics and binding free-energy calculations demonstrated substantially reduced macrolide affinity following the A2058G mutation.
- **Dissemination Dynamics:** Integrated genomic surveillance confirmed widespread mobile-element-mediated resistance dissemination across diverse pathogenic lineages.



ABSTRACT

Background: Antimicrobial resistance (AMR) is a major global public health challenge, with particularly important consequences in settings where antibiotic use, diagnostic capacity, and antimicrobial stewardship remain heterogeneous. Macrolides are widely used for community-acquired respiratory and skin and soft-tissue infections, but increasing resistance threatens their therapeutic effectiveness. Genomic surveillance data describing the molecular basis and dissemination of macrolide resistance in Egyptian primary healthcare settings remain limited.

Methods: A multicenter cross-sectional investigation was conducted from January to December 2023 across 15 primary healthcare facilities in three Egyptian governorates: Cairo, Alexandria, and Assiut. A total of 842 clinical specimens were collected from patients presenting with suspected bacterial respiratory or skin and soft-tissue infections. Bacterial isolates were identified using matrix-assisted laser desorption/ionization time-of-flight mass spectrometry, and antimicrobial susceptibility testing was performed according to CLSI M100-Ed34 (2024). Macrolide-resistant isolates were subjected to genomic characterization using Oxford Nanopore MinION and Pacific Biosciences Sequel IIe sequencing platforms. Resistance determinants, plasmids, integrative conjugative elements, sequence types, and phylogenetic relationships were investigated using established antimicrobial-resistance and genome-analysis databases and bioinformatic pipelines. Targeted PacBio HiFi sequencing was additionally used to characterize 23S rRNA mutations.

Results: Among 642 confirmed bacterial pathogens, 289 (45.0%, 95% CI: 41.2–48.9%) exhibited phenotypic macrolide resistance. Resistance was highest among Staphylococcus aureus (58.2%, 114/196), followed by Streptococcus pneumoniae (45.0%, 98/218), Streptococcus pyogenes (39.7%, 62/156), and Haemophilus influenzae (20.8%, 15/72). The ermB gene predominated among resistant streptococci, occurring in 81.6% of resistant S. pneumoniae and 80.6% of resistant S. pyogenes isolates, whereas ermC predominated among resistant S. aureus isolates (87.7%, 100/114). Long-read sequencing enabled reconstruction of 45 plasmids and 12 integrative conjugative elements associated with resistance determinants. A conserved ermC-carrying plasmid, designated pEC-Egy1 (3,142 bp), was detected in

68.0% of ermC-positive S. aureus isolates across the three governorates, with 99.8% sequence identity among detected variants. PacBio HiFi sequencing identified the A2058G 23S rRNA mutation in 22/289 resistant isolates (7.6%) and revealed mixed wild-type and mutant alleles consistent with heteroresistance in 9/289 isolates (3.1%). Heteroresistant isolates exhibited lower erythromycin MICs (4–16 μg/mL) than isolates carrying predominantly homogeneous A2058G mutant populations (32–128 μg/mL; $p<0.001$). Phylogenomic analysis showed that CC320 represented 36.7% of resistant S. pneumoniae isolates, whereas the pEC-Egy1 plasmid occurred across multiple S. aureus sequence types.

Conclusion: Integrated third-generation sequencing provided high-resolution characterization of macrolide resistance determinants, their genomic contexts, and dissemination patterns among bacterial pathogens from Egyptian primary healthcare facilities. The findings demonstrate the coexistence of clonal dissemination and horizontal mobility of resistance determinants and highlight the value of long-read sequencing for resolving plasmid structures, mobile genetic elements, and heterogeneous 23S rRNA resistance alleles. These genomic data provide a framework for continued molecular surveillance of macrolide resistance in Egyptian primary healthcare settings.

Keywords: Antimicrobial Resistance; Macrolides; Egypt; Primary Healthcare; Third-Generation Sequencing; Oxford Nanopore Technologies; Pacific Biosciences; Molecular Epidemiology; Horizontal Gene Transfer; ermB; ermC; Heteroresistance; 23S rRNA Mutation

1. INTRODUCTION

Antimicrobial resistance (AMR) is a major and rapidly evolving global public-health challenge, with substantial consequences for morbidity, mortality, healthcare expenditure, and the effectiveness of antimicrobial therapy. The global burden of bacterial AMR has been estimated to account for millions of deaths annually, while the continued expansion of resistant bacterial populations is expected to increase the clinical and economic burden over the coming decades (1,2). Among antimicrobial classes, macrolides remain important therapeutic agents because of their activity against a broad range of Gram-positive and selected Gram-negative bacterial pathogens. Erythromycin, azithromycin, and clarithromycin are widely used for the treatment of respiratory tract infections and selected skin and soft-tissue infections, particularly when β-lactam therapy is contraindicated or ineffective (3,4).

Macrolide resistance is increasingly reported among clinically important respiratory and skin-associated bacterial pathogens. In Streptococcus pneumoniae, Streptococcus pyogenes, and Staphylococcus aureus, resistance may substantially reduce the effectiveness of commonly prescribed macrolide-based regimens and may coexist with resistance to other antimicrobial classes (5). The molecular basis of macrolide resistance is diverse and includes target-site modification, active drug efflux, and chromosomal alterations affecting the ribosomal target. The most important acquired mechanisms include methylation of the 23S rRNA mediated by erm genes, active efflux mediated by mef determinants, and the contribution of additional resistance-associated genes such as msr. Mutations within the 23S rRNA and genes encoding ribosomal proteins L4 and L22 can further modify macrolide binding and contribute to high-level or altered resistance phenotypes (5,6).

Egypt faces several challenges in controlling antimicrobial resistance, including inappropriate antimicrobial use, non-prescription access to antibiotics, variable antimicrobial stewardship practices, and limited availability of rapid microbiological diagnostics in some healthcare settings (7,8). These factors may contribute to the selection and persistence of resistant bacterial populations within community and primary healthcare environments. Primary healthcare centers are particularly important surveillance settings because they represent an early point of contact between patients and the healthcare system and therefore provide an opportunity to identify emerging resistance patterns before they become established across broader healthcare networks. Genomic surveillance in these settings can complement conventional antimicrobial susceptibility testing by identifying the genetic determinants and mobile elements responsible for resistance dissemination.

Conventional molecular approaches have provided important information about individual resistance genes; however, targeted detection alone may not adequately resolve the genomic organization, mobility, or evolutionary relationships of resistance determinants. Mobile genetic elements, including plasmids, transposons, integrative conjugative elements (ICEs), and other horizontally transferable DNA structures, can facilitate the movement of resistance genes between bacterial strains and, in some circumstances, between species (6,13,14). Determining whether resistance determinants occur within conserved chromosomal regions, plasmids, transposons, or ICEs is therefore essential for understanding their potential for dissemination. Long-read sequencing provides an important advantage in this context because it can span repetitive regions and complex resistance-associated loci that may remain fragmented in short-read assemblies.

Third-generation sequencing platforms, particularly Oxford Nanopore Technologies (ONT) and Pacific Biosciences (PacBio) sequencing, provide long DNA reads that can facilitate reconstruction of bacterial

chromosomes, plasmids, repetitive regions, and mobile geneticelements. ONT sequencing can generate long reads in real time, whereas PacBio HiFi sequencing provides highly accurate long reads suitable for resolving complex genomic structures and detecting sequence variants with high confidence. The combination of these technologies can therefore provide complementary information for bacterial genome assembly, resistance-gene characterization, plasmid reconstruction, and investigation of horizontal gene transfer (9,10,14).

Genomic approaches are also particularly valuable for investigating resistance phenotypes that may not be fully explained by conventional susceptibility testing. Heteroresistance, for example, describes the presence of subpopulations with different antimicrobial susceptibility profiles within an apparently homogeneous bacterial population and can complicate therapeutic decision-making and laboratory interpretation (12). Long-read sequencing and targeted high-fidelity sequencing of resistance-associated loci may help identify low-frequency or minority resistance variants that could otherwise remain undetected by routine approaches.

Despite increasing availability of antimicrobial-resistance surveillance data, detailed genomic characterization of macrolide-resistant pathogens from Egyptian primary healthcare settings remains limited. In particular, information is needed regarding the distribution of major macrolide-resistance determinants, their genomic contexts, the contribution of plasmids and ICEs to their dissemination, the population structure of resistant pathogens, and the relationship between specific mutations and phenotypic resistance levels. Integrating phenotypic antimicrobial susceptibility testing with long-read genome sequencing, comparative genomics, and molecular-dynamics analysis may provide a more comprehensive view of these processes.

Therefore, the present study investigated the molecular epidemiology and genomic architecture of macrolide resistance among bacterial pathogens recovered from primary healthcare centers in three major Egyptian regions. The study integrated conventional microbiological characterization with third-generation sequencing using ONT and PacBio platforms to identify resistance determinants, reconstruct resistance-associated mobile genetic elements, characterize bacterial population structure, and investigate geographic patterns of dissemination. Targeted sequencing of the 23S rRNA locus was additionally used to characterize resistance-associated mutations and heteroresistant populations. Finally, structural and molecular-dynamics analyses were performed to investigate the potential effects of the A2058G substitution on macrolide–ribosomal interactions. This integrated approach was intended to provide high-resolution genomic evidence relevant to antimicrobial-resistance surveillance and the development of more informed stewardship and infection-control strategies in Egyptian primary healthcare settings.

1. INTRODUCTION

Antimicrobial resistance (AMR) has become a major global threat to the effective treatment of bacterial infections. Resistant bacterial infections are associated with substantial morbidity and mortality and increasingly compromise the effectiveness of commonly used antimicrobial agents. A comprehensive global analysis estimated that bacterial AMR was directly attributable to approximately 1.27 million deaths in 2019, emphasizing the need for strengthened surveillance, prevention, antimicrobial stewardship, and development of effective therapeutic strategies [1]. In response to the expanding threat, the World Health Organization (WHO) established the Global Action Plan on Antimicrobial

Resistance, identifying surveillance, infection prevention, optimized antimicrobial use, research, and development of new interventions as major priorities for controlling AMR [2].

Pharmacological Background and Clinical Utility of Macrolides

Macrolides constitute an important class of antibacterial agents used particularly for respiratory tract infections and infections caused by Gram-positive organisms. However, increasing macrolide resistance has progressively reduced their clinical utility in several bacterial pathogens. Global surveillance data indicate substantial geographic and temporal variation in macrolide and macrolide-associated resistance, highlighting the importance of continuous regional monitoring [3]. Azithromycin and erythromycin exert their antibacterial activity predominantly through interaction with the bacterial 50S ribosomal subunit, where they interfere with protein synthesis and inhibit bacterial growth. Their pharmacological characteristics and broad clinical applications have contributed to their extensive use in human medicine [4].

Molecular Mechanisms of Macrolide Resistance

Bacterial resistance to macrolides can arise through several molecular mechanisms. These include modification of the ribosomal target by erm-encoded methyltransferases, active antimicrobial efflux mediated by mef and associated systems, and nucleotide substitutions within the 23S rRNA that alter the macrolide-binding environment. In Streptococcus pneumoniae, erm(B)-mediated target modification and mef(A/E)-associated efflux represent important mechanisms, while combinations of resistance mechanisms may produce substantially different levels of phenotypic resistance [5]. The genetic organization of these determinants is particularly important because resistance genes can occur within transposons and other mobile elements capable of facilitating their movement among bacterial populations. The mobility of erm(B)-associated elements has been demonstrated in clinically important streptococci, emphasizing the importance of characterizing resistance genes together with their surrounding genomic contexts [6].

Epidemiological Drivers and One Health Perspective

The epidemiology of AMR is influenced by antimicrobial consumption, prescribing practices, healthcare infrastructure, infection-control measures, and population-level transmission. In Egypt, studies of antibiotic use have identified practices and stewardship-related factors that may contribute to inappropriate antimicrobial exposure and consequently to the selection and persistence of resistant organisms [7]. The Egyptian AMR situation is also influenced by interactions among human, animal, and environmental reservoirs, supporting the application of a One Health perspective to surveillance and control strategies [8]. Nevertheless, molecularly resolved surveillance data from primary healthcare settings remain comparatively limited, particularly for macrolide-resistant bacterial pathogens.

Genomic Surveillance and Long-Read Sequencing Technologies

Conventional AMR surveillance generally combines bacterial culture, antimicrobial susceptibility testing, and targeted molecular detection of established resistance genes. These approaches remain essential

for clinical microbiology but may fail to identify resistance mechanisms outside predefined targets or to resolve the genomic context in which resistance determinants occur. Genome-based approaches can overcome several of these limitations by simultaneously characterizing resistance genes, chromosomal mutations, plasmids, mobile genetic elements, sequence types, and broader genomic relationships. Contemporary computational approaches increasingly integrate resistome analysis with genome assembly, annotation, comparative genomics, and prediction of resistance phenotypes, providing a more comprehensive framework for AMR characterization [9].

Third-generation sequencing technologies provide additional advantages for bacterial genomic epidemiology because of their capacity to generate long sequencing reads. Oxford Nanopore Technologies (ONT) sequencing can facilitate reconstruction of repetitive genomic regions and complex mobile genetic elements, whereas PacBio HiFi sequencing combines long-read sequencing with high per-base accuracy and is particularly useful for resolving complete genomic structures and nucleotide-level variants. Comparative evaluations of long-read sequencing have demonstrated its utility for bacterial genome reconstruction and antimicrobial-resistance characterization [10]. Integration of genomic sequencing with established international surveillance frameworks can further strengthen the identification and tracking of resistance determinants across healthcare systems and geographic regions [11].

Heteroresistance and Horizontal Gene Transfer

An additional challenge in antimicrobial susceptibility surveillance is heteroresistance, in which genetically or phenotypically distinct subpopulations with different antimicrobial susceptibility profiles coexist within an apparently homogeneous bacterial population. Conventional susceptibility testing may overlook minority resistant populations when they constitute only a fraction of the total population. Under antimicrobial selection pressure, these subpopulations may expand and become clinically relevant, making heteroresistance an important consideration in the interpretation of antimicrobial susceptibility and genomic data [12].

The dissemination of antimicrobial resistance is further facilitated by horizontal gene transfer. Plasmids, transposons, integrative and conjugative elements (ICEs), insertion sequences, and other mobile genetic elements can capture, maintain, and transfer resistance determinants between bacterial cells. Clinical environments provide opportunities for the exchange of resistance genes among bacterial populations, potentially contributing to the persistence and spread of multidrug-resistant organisms [13]. Genome-resolved mobilome analyses have consequently become increasingly important for determining whether resistance determinants are chromosomal or mobile and for identifying the genetic structures associated with their dissemination [14].

Standardized Testing and Study Rationale

Standardized antimicrobial susceptibility testing remains an essential component of AMR surveillance and provides the phenotypic framework against which genomic findings can be interpreted. The Clinical and Laboratory Standards Institute (CLSI) provides standardized procedures and interpretive criteria for

antimicrobial susceptibility testing, enabling consistent classification of bacterial isolates and comparison of resistance phenotypes across studies and surveillance settings [15].

Despite advances in genomic surveillance, integrated molecular epidemiological characterization of macrolide-resistant bacterial pathogens in Egyptian primary healthcare settings remains limited. In particular, there is a need to connect phenotypic susceptibility profiles with specific resistance determinants, 23S rRNA mutations, plasmids, integrative and conjugative elements, sequence types, and whole-genome phylogenetic relationships. Such integration can help distinguish dominant resistance mechanisms from less readily detectable variants and clarify the genomic contexts in which resistance determinants occur.

The present study investigated the molecular epidemiology and resistance profiles of macrolide-resistant bacterial pathogens recovered from primary healthcare centers in Cairo, Alexandria, and Assiut, Egypt. The study integrated conventional microbiological characterization with antimicrobial susceptibility testing, targeted molecular analysis, ONT long-read sequencing, PacBio HiFi sequencing, targeted 23S rRNA sequencing, resistome profiling, plasmid and mobile-element analysis, multilocus sequence typing, and whole-genome phylogenetics. The study also evaluated the molecular consequences of the A2058G 23S rRNA mutation using molecular-dynamics simulations, binding free-energy calculations, residue-level interaction analysis, and potential-of-mean-force analysis. Collectively, this approach was designed to provide a high-resolution characterization of macrolide resistance mechanisms, their genomic contexts, their distribution among bacterial lineages, and their epidemiological patterns in Egyptian primary healthcare settings.

2. MATERIALS AND METHODS

> *Methodology Protocol&Experimental Design Guidelines*
> *Multicenter Cross-Sectional Study on Macrolide Resistance Determinants and Molecular Dynamics*

2.1 Study Design and Clinical Sampling

A multicenter cross-sectional study was conducted from January to December 2023 across 15 primary healthcare centers (PHCs) located in Cairo, Alexandria, and Assiut, Egypt. Patients presenting with clinically suspected respiratory tract infections, including pharyngitis, pneumonia, and acute otitis media, or skin and soft-tissue infections, including abscesses and cellulitis, were consecutively enrolled.

The target sample size was initially estimated at 750 specimens using an anticipated macrolide-resistance prevalence of 15%, a 5% margin of error, and a 95% confidence level, with an additional adjustment for clustering among participating healthcare centers. During the study period, 842 clinical specimens were collected, including throat swabs, sputum samples, and pus swabs.

Specimens were transported to the microbiology laboratory within 2 h of collection under appropriate conditions and processed immediately upon receipt.

The study protocol was reviewed and approved by the Institutional Review Board of the Faculty of Pharmacy, Cairo University (CU-FOP-IRB-2023-0456). The study was conducted in accordance with the ethical principles of the Declaration of Helsinki (2013) and applicable Egyptian Ministry of Health and Population requirements. Written informed consent was obtained from adult participants or their legal representatives. For participants aged 7–17 years, age-appropriate assent was obtained in addition to parental or legal-guardian consent.

2.2 Bacterial Isolation and Identification

Throat and pus specimens were inoculated onto 5% sheep-blood agar prepared from Blood Agar Base (Oxoid, Thermo Fisher Scientific, OXCM0055B) and Columbia CNA agar (BD, 212104). Sputum specimens were initially evaluated by Gram staining, and specimens demonstrating acceptable quality, defined as ≥25 leukocytes and ≤10 epithelial cells per low-power field, were processed for bacterial culture.

Sputum specimens were inoculated onto chocolate agar (BD, B21169X) and MacConkey agar (Oxoid, UK). Plates were incubated at 35 ± 2°C for 24–48 h, with fastidious organisms incubated in an atmosphere containing 5% CO_2 when required. Colonies displaying characteristic morphology were subjected to species-level identification using matrix-assisted laser desorption/ionization time-of-flight mass spectrometry (MALDI-TOF MS; Bruker Biotyper, Bruker Daltonics, bacterial test standard 8255343). Identification scores ≥2.0 were accepted for reliable species-level identification.

2.3 Antimicrobial Susceptibility Testing

Antimicrobial susceptibility testing (AST) was performed using the Kirby–Bauer disk-diffusion method on Mueller–Hinton agar (Oxoid, CM0337B). For fastidious organisms, Mueller–Hinton agar supplemented with 5% sheep blood was used. Bacterial suspensions were adjusted to a 0.5 McFarland standard before inoculation.

The macrolide agents tested were erythromycin (15 µg; Oxoid, CT0020B), azithromycin (15 µg; Oxoid, CT0642B), and clindamycin (2 µg; Oxoid, CT0064B). Zone diameters were interpreted according to the Clinical and Laboratory Standards Institute (CLSI) M100, 34th edition (2024). For erythromycin, isolates were classified as susceptible at inhibition zones ≥23 mm, intermediate at 14–22 mm, and resistant at ≤13 mm. For azithromycin, susceptible isolates demonstrated zones ≥18 mm, intermediate isolates 14–17 mm, and resistant isolates ≤13 mm. For clindamycin, susceptible isolates demonstrated zones ≥21 mm, intermediate isolates 15–20 mm, and resistant isolates ≤14 mm. Because standardized erythromycin breakpoints were not applied to Haemophilus influenzae in this study, azithromycin susceptibility was used for macrolide-resistance characterization in this species.

Minimum inhibitory concentrations (MICs) were additionally determined using E-test strips (bioMérieux, 501518). E-test assays were incubated at 35 ± 2°C for 24 h, with 5% CO_2 used for

fastidious organisms. Streptococcus pneumoniae ATCC 49619 and Staphylococcus aureus ATCC 29213 were included as quality-control strains.

2.4 Phenotypic Characterization of Macrolide Resistance

Macrolide–lincosamide–streptogramin B (MLS_B) resistance phenotypes were characterized using the double-disk D-zone test. Erythromycin and clindamycin disks were placed 15–20 mm edge-to-edge on the inoculated agar surface. After incubation, isolates resistant to erythromycin and clindamycin without flattening of the clindamycin inhibition zone were classified as constitutive MLS_B (cMLS_B). Isolates resistant to erythromycin but susceptible to clindamycin and showing a D-shaped zone adjacent to the erythromycin disk were classified as inducible MLS_B (iMLS_B).

Isolates exhibiting macrolide resistance while remaining susceptible to clindamycin and lacking inducible flattening were classified according to the corresponding macrolide-efflux phenotype. The phenotypic classifications were subsequently compared with the resistance determinants identified by genomic analysis.

2.5 PCR-Based Screening of Macrolide-Resistance Determinants

All phenotypically macrolide-resistant isolates were screened for major acquired macrolide-resistance determinants, including ermA, ermB, ermC, mefA, mefE, and msrA, together with the 23S rRNA locus.

The following primer sets and expected amplicon sizes were used:

Target	Forward primer (5′–3′)	Reverse primer (5′–3′)	Expected size
ermA	TCTAAAAAGCATGTAAAAGAA	CTTCGATAGTTTATTAATATTAGT	645 bp
ermB	GAAAAGGTACTCAACCAAATA	AGTAACGGTACTTAAATTGTTTAC	639 bp
ermC	TCAAAACATAATATAGATAAA	GCTAATATTGTTTAAATCGTCAAT	572 bp
mefA	AGTATCATTAATCACTAGTGC	TTCTTCTGGTACTAAAAGTGG	346 bp
mefE	GACCGAATTAGGCAGCAT	CAATTCCAGAGCAGCA	403 bp
msrA	GGCACAATAAGAGTGTTTAA	AAGTTATATCATGAATAGATTGTCC TGTT	399 bp
23S rRNA	AGAGTTTGATCMTGGCTCAG	ACGGYTACCTTGTTACGACTT	~5,500 bp

PCR assays were evaluated using appropriate positive and negative controls. The assays demonstrated reported analytical specificity of 100%, with observed amplification products corresponding to the expected target sizes. Calculated PCR efficiencies ranged from 95.4% to 99.1%.

2.6 High-Molecular-Weight DNA Extraction

Genomic DNA was extracted using the MagAttract HMW DNA Kit (Qiagen, 67563). Bacterial biomass was initially collected by centrifugation at 5,000 × g for 10 min at room temperature. The pellet was resuspended in 180 µL ATL buffer supplemented with 20 µL lysozyme (10 mg/mL; Sigma-Aldrich, L6876) and 5 µL lysostaphin (2 mg/mL; Sigma-Aldrich, L7386). The suspension was incubated at 37°C for 30 min with gentle shaking to facilitate cell-wall disruption.

Protein digestion was subsequently performed by adding 25 µL proteinase K and 200 µL AL buffer followed by incubation at 56°C for 30 min. Magnetic-bead purification was then performed according to the manufacturer's protocol. DNA was finally eluted in 100 µL AE buffer prewarmed to 65°C.

DNA concentration was measured using the Qubit dsDNA Broad Range Assay (Q32853) and a Qubit 4 fluorometer (Q33238). For quantification, 2 µL DNA was combined with 198 µL working solution prepared at a 1:200 reagent dilution and incubated for 2 min before measurement.

DNA integrity was initially assessed by electrophoresis on 0.6% agarose prepared in 1× TAE buffer at 5 V/cm for 60 min. Representative high-molecular-weight DNA preparations were further evaluated using the Agilent TapeStation system with the Genomic DNA12000 kit (5067-1508) on an Agilent 4150 instrument. DNA preparations with an estimated fragment size >20 kb and an A260/A280 ratio of 1.8–2.0 were selected for long-read sequencing.

2.7 Oxford Nanopore Long-Read Sequencing

For Oxford Nanopore Technologies (ONT) sequencing, 400 ng of high-molecular-weight genomic DNA was processed using the SQK-LSK114 ligation sequencing kit and NEBNext Companion Module (E7180S). DNA repair and end-preparation were performed in a 48-µL reaction containing 3.5 µL FFPE DNA repair buffer, 2 µL repair mix, 3.5 µL Ultra II end-preparation buffer, and 3 µL end-preparation enzyme. The reaction was incubated at 20°C for 5 min followed by 65°C for 5 min.

The resulting DNA was purified using 60 µL AMPure XP beads followed by washing with 70% ethanol and elution in 61 µL nuclease-free water. For adapter ligation, 60 µL prepared DNA was combined with 25 µL LNB, 10 µL Quick T4 DNA ligase (M0202), and 5 µL ligation adapter and incubated at room temperature for 10 min. The ligation product was purified using 40 µL AMPure beads, washed using LFB buffer, and eluted in 15 µL EB buffer. Final library concentration was determined using the Qubit high-sensitivity assay.

Libraries were sequenced on a MinION Mk1C device (MIN-101C) equipped with R10.4.1 flow cells (FLO-MIN114). Sequencing was performed for up to 72 h using active-channel selection and the super-accurate basecalling configuration implemented in MinKNOW v22.08.6.

2.8 PacBio HiFi Sequencing

For PacBio sequencing, 1 µg of high-molecular-weight genomic DNA was used for library construction with the SMRTbell Prep Kit 3.0 (102-182-700). DNA was mechanically sheared to an approximate fragment size of 15 kb using a Megaruptor 3 system (B06010003/E07010003). Size selection was performed using a 0.75% BluePippin cassette (BLF7510) with a 10-kb cutoff.

DNA repair, end repair, and adapter ligation were performed according to the SMRTbell library-preparation workflow, followed by bead-based cleanup. Final libraries were quantified using Qubit and assessed for fragment-size distribution using a Femto Pulse system.

Sequencing was performed on a PacBio Sequel IIe instrument using one 8M SMRT Cell per library. Sequencing movies were collected for 30 h, and circular consensus sequencing (CCS) analysis was used to generate high-fidelity (HiFi) reads. Sequencing was performed using Sequel II Sequencing Kit 2.0 (101-820-200) and Sequel II Binding Kit 2.2 (101-908-100).

2.9 Targeted 23S rRNA Sequencing

Targeted sequencing of the 23S rRNA locus was performed for isolates requiring additional characterization of macrolide-resistance-associated mutations. Amplification was performed using PrimeSTAR GXL DNA Polymerase (Takara, R050A) and the universal 23S rRNA primers listed above.

Each 50-µL PCR reaction contained 10 µL of 5× reaction buffer, 4 µL dNTP mixture (2.5 mM each), 1 µL of each primer (20 µM), 1 µL PrimeSTAR GXL polymerase (1.25 U/µL), 2 µL template DNA at 50 ng, and 31 µL nuclease-free water. Amplification consisted of an initial denaturation at 98°C for 2 min, followed by 35 cycles of 98°C for 10 s, 55°C for 15 s, and 68°C for 6 min, with a final extension at 68°C for 10 min. The expected product was approximately 5.5 kb.

Amplified products were purified using AMPure PB beads at a 1:1 bead-to-sample ratio and subsequently processed for SMRTbell 3.0 library preparation. Sequencing was performed on the Sequel IIe platform using 30-h sequencing movies. HiFi reads with a predicted quality value >Q20 were retained for downstream analysis.

2.10 Long-Read Processing and Genome Assembly

ONT reads were adapter-trimmed using Porechop v0.2.4 and evaluated using NanoPlot v1.32.1. High-quality ONT reads were assembled using Flye v2.9.6 with the '--nano-hq' option. PacBio HiFi reads were assembled using hifiasm v0.16.1.

Assembly quality was assessed using QUAST v5.0.2, while genome completeness and contamination were evaluated using CheckM v1.1.3. The resulting assemblies were subsequently inspected for chromosome and plasmid structure and manually reviewed where necessary.

The sequencing dataset generated approximately 45.2 Gb of ONT raw data, with a mean read length of 12.4 kb and a read N50 of 18.6 kb. ONT assemblies contained a mean of 3.2 contigs, with a mean contig N50 of 2.1 Mb and estimated completeness of 99.2%. PacBio sequencing generated approximately 38.7 Gb of data, with a mean read length of 15.2 kb and a read N50 of 14.8 kb. PacBio

assemblies contained a mean of 2.1 contigs, with a mean contig N50 of 2.6 Mb and estimated completeness of 99.5%. The mean assembled genome size was approximately 2.8 Mb, with an overall GC content of approximately 38.2%.

2.11 Genome Annotation and Resistance-Gene Identification

Genome annotation was performed using Prokka v1.14.6. Multilocus sequence types (MLSTs) were determined using mlst v2.0 against the PubMLST databases.

Antimicrobial-resistance determinants were identified using ABRicate v1.0.1 against the Comprehensive Antibiotic Resistance Database (CARD) v3.2.8 and ResFinder v4.0. Resistance-gene hits were retained using a minimum sequence identity of 90% and minimum coverage of 80%. Chromosomal point mutations associated with antimicrobial resistance were additionally investigated using PointFinder.

Plasmid-associated sequences were identified using PlasmidFinder v2.1 with minimum identity and coverage thresholds of 95% and 60%, respectively. Integrative conjugative elements were investigated using ICEfinder v2.0, while additional mobile genetic elements were characterized using MobileElementFinder.

Resistance-associated genomic regions were manually inspected to determine the organization of resistance genes, transposases, recombination-associated genes, replication-associated genes, mobilization genes, and conjugation-associated loci.

2.12 Comparative Genomics and Phylogenetic Analysis

Core-genome multilocus sequence typing (cgMLST) was performed using chewBBACA v2.8.0. The analysis included 1,861 core genes for S. aureus and 1,605 core genes for S. pneumoniae. Core-genome single-nucleotide polymorphisms were identified and used for phylogenetic reconstruction.

Maximum-likelihood phylogenies were generated using RAxML v8.2.12 under the GTRGAMMA substitution model with 100 bootstrap replicates. Phylogenetic trees were subsequently visualized and annotated using iTOL v6. Geographic metadata, sequence types, resistance determinants, and mobile-element information were integrated into the resulting trees.

Plasmid and mobile-element structures were further examined using Bandage v0.8.1. Comparative analysis of mobile genetic elements was performed using reference information from ACLAME and ICEberg databases.

2.13 Statistical Analysis

Statistical analyses were performed using R version 4.2.0. Categorical variables were summarized as frequencies and percentages, while continuous variables were summarized using means and standard deviations or medians and ranges as appropriate. Exact or asymptotic 95% confidence intervals were calculated for resistance proportions.

Associations between categorical variables were evaluated using the chi-square test or Fisher's exact test when expected cell counts were insufficient for chi-square analysis. Differences in continuous variables between groups were assessed using the Kruskal–Wallis test where appropriate. Correlation analyses were performed for genomic and phenotypic resistance measurements. Multiple-comparison correction was performed using the Benjamini–Hochberg procedure. A two-sided p value<0.05 was considered statistically significant.

2.14 Molecular-Dynamics Simulation of the 23S rRNA–Macrolide Complex

The structural consequences of the A2058G 23S rRNA substitution were investigated using molecular-dynamics (MD) simulations. Structural models of the 23S rRNA domain V were derived from experimentally determined ribosomal structures available in the Protein Data Bank, including PDB entries 1JZY and 4V7X. Homology models representing the corresponding S. pneumoniae and S. aureus ribosomal environments were generated using SWISS-MODEL.

The A2058G substitution was introduced using PyMOL v2.5. Residue numbering was interpreted according to the corresponding bacterial 23S rRNA nomenclature; the equivalent position is reported as A2059 in some bacterial numbering systems.

Erythromycin and azithromycin structures were obtained from experimentally resolved structural information and prepared for simulation. The CHARMM General Force Field (CGenFF) was used for the macrolactone and desosamine-containing ligand components, while RESP-derived partial charges were generated using Antechamber. RNA parameters were assigned using an AMBER RNA force-field framework incorporating the χOL3 correction.

Each simulation system contained approximately 500 nucleotides. Systems were solvated in a truncated-octahedral TIP3P water box with a minimum 12 Å solvent buffer and neutralized with Na^+ and Cl^- ions to a final ionic strength of 0.15 M using Joung–Cheatham ion parameters.

The four principal simulation systems comprised wild-type 23S rRNA bound to erythromycin, A2058G-mutant 23S rRNA bound to erythromycin, wild-type 23S rRNA bound to azithromycin, and A2058G-mutant 23S rRNA bound to azithromycin. The erythromycin wild-type system contained 502 rRNA residues, one ligand, 28,456 water molecules, 142 Na^+ ions, 138 Cl^- ions, and 89,234 atoms. The corresponding mutant system contained 28,234 water molecules, 141 Na^+ ions, 137 Cl^- ions, and 88,876 atoms. The wild-type azithromycin system contained 28,892 water molecules, 143 Na^+ ions, 139 Cl^- ions, and 90,456 atoms, whereas the mutant azithromycin system contained 28,678 water molecules, 142 Na^+ ions, 138 Cl^- ions, and 89,987 atoms.

MD simulations were performed using GROMACS 2023.1 on NVIDIA A100 GPU hardware. The AMBER99SB-ILDN force field was applied to protein components where present, while CHARMM36 parameters were used for nucleic-acid and ligand components according to the prepared parameterization scheme.

Energy minimization consisted of 5,000 steps of steepest descent followed by 5,000 steps of conjugate-gradient minimization. Systems were subsequently heated from 0 to 310 K over 500 ps using a velocity-rescaling thermostat with a coupling constant of 0.1 ps while positional restraints were maintained at 10 kcal/mol/$Å^2$. Equilibration under NPT conditions was performed at 1 bar

using a Parrinello–Rahman barostat with a 2-ps coupling constant. Positional restraints were progressively reduced from 10 kcal/mol/Å^2 to zero during the first 1 ns of equilibration.

Production simulations were performed for 500 ns using a leap-frog integration algorithm and a 2-fs time step. Hydrogen-containing bonds were constrained using LINCS. Long-range electrostatic interactions were calculated using the Particle Mesh Ewald method with a 10 Å real-space cutoff. van der Waals interactions were treated using a 10 Å cutoff with switching beginning at 8 Å. Three independent replicas were generated for each system, resulting in a total simulation time of 6 μs.

2.15 MM/PBSA Binding Free-Energy Analysis

Molecular-mechanics/Poisson–Boltzmann surface-area (MM/PBSA) calculations were performed using gmx_MMPBSA. A total of 5,000 snapshots were extracted from the final 100 ns of each trajectory at 20-ps intervals.

Binding free energy was calculated according to:
$\Delta G_{bind} = G_{complex} - (G_{receptor} + G_{ligand})$

where the total free energy was represented as:
$G = E_{MM} + G_{solv} - T\Delta S$

The resulting binding-energy components were compared between wild-type and A2058G-mutant systems to estimate the energetic contribution of the mutation to macrolide binding.

2.16 Umbrella-Sampling Analysis

Umbrella-sampling simulations were performed to characterize the free-energy profile associated with ligand dissociation. Thirty windows spanning a 0–30 Å reaction coordinate were generated. The potential of mean force (PMF) was subsequently reconstructed from the umbrella-sampling trajectories using the weighted histogram analysis method (WHAM).

The resulting PMF profiles were compared between wild-type and A2058G-mutant complexes to assess differences in the energetic landscape associated with macrolide retention and dissociation from the 23S rRNA binding site.

2.17 Molecular-Dynamics Statistical Analysis

Trajectory-derived structural and energetic parameters were expressed as mean ± standard deviation across independent replicates.

RESULTS

3.1 Study Population and Bacterial Recovery

A total of 842 clinical specimens were collected from patients attending 15 primary healthcare centers in Cairo, Alexandria, and Assiut during the study period. Bacterial pathogens were recovered from 642 specimens, corresponding to an overall culture positivity rate of 76.2%. The study population comprised

456 male participants (54.2%) and 386 female participants (45.8%), with a mean age of 34.7 ± 18.2 years (range, 1–78 years).

Throat swabs represented the largest specimen category, accounting for 412 specimens (48.9%), followed by sputum samples from 268 patients (31.8%) and pus swabs from 162 patients (19.3%). Among the 642 confirmed bacterial isolates, S. pneumoniae accounted for 218 isolates, S. pyogenes for 156, S. aureus for 196, and H. influenzae for 72 isolates (Table 1).

The distribution of specimens and confirmed bacterial isolates was broadly comparable among the three geographic regions. Cairo contributed 286 specimens, Alexandria 298, and Assiut 258. The corresponding numbers of confirmed bacterial isolates were 214, 228, and 200, respectively (Table 1).

3.2 Prevalence and Geographic Distribution of Macrolide Resistance

Among the 642 confirmed bacterial isolates, 289 were classified as macrolide resistant, giving an overall resistance prevalence of 45.0% (95% CI, 41.2–48.9%). Resistance was highest among S. aureus, with 114 of 196 isolates resistant (58.2%; 95% CI, 51.2–65.0%), followed by S. pneumoniae with 98 of 218 isolates (45.0%; 95% CI, 38.5–51.6%), S. pyogenes with 62 of 156 isolates (39.7%; 95% CI, 32.4–47.5%), and H. influenzae with 15 of 72 isolates (20.8%; 95% CI, 13.0–31.5%) (Table 1).

Resistance prevalence varied modestly between geographic regions. Among S. pneumoniae, resistance was detected in 32/75 isolates (42.7%) from Cairo, 38/78 (48.7%) from Alexandria, and 28/65 (43.1%) from Assiut. Corresponding values for S. pyogenes were 34.6%, 41.4%, and 43.5%, respectively. Among S. aureus, resistance was observed in 35/64 isolates (54.7%) from Cairo, 42/70 (60.0%) from Alexandria, and 37/62 (59.7%) from Assiut. H. influenzae resistance was 17.4%, 27.3%, and 18.5% in Cairo, Alexandria, and Assiut, respectively (Table 2).

Overall resistance among all bacterial isolates was 89/214 (41.6%) in Cairo, 110/228 (48.2%) in Alexandria, and 90/200 (45.0%) in Assiut. The geographic difference was not statistically significant ($p = 0.083$).

3.3 Seasonal and Clinical Distribution of Resistance

Macrolide resistance showed no significant seasonal variation. Resistance was detected in 82/168 isolates (48.8%) during winter, 68/156 (43.6%) during spring, 72/162 (44.4%) during summer, and 67/156 (42.9%) during autumn ($p = 0.67$).

Resistance prevalence was also similar across the major clinical presentations. The proportions of resistant isolates were 82/186 (44.1%) among patients with pharyngitis, 68/142 (47.9%) among those with pneumonia, 42/98 (42.9%) among patients with acute otitis media, 58/124 (46.8%) among patients with abscesses, and 39/92 (42.4%) among patients with cellulitis. No significant association was observed between clinical presentation and resistance status ($p = 0.82$).

3.4 Macrolide-Resistance Phenotypes

Phenotypic characterization of the 289 macrolide-resistant isolates identified 234 isolates (81.0%) with constitutive MLS_B (cMLS_B) resistance, 17 (5.9%) with inducible MLS_B (iMLS_B), 23 (8.0%) with an M phenotype, and 15 (5.2%) with an MS phenotype (Table 3).

Among S. pneumoniae, 78/98 resistant isolates (79.6%) exhibited cMLS_B, 8 (8.2%) iMLS_B, and 12 (12.2%) an M phenotype. Among S. pyogenes, the corresponding values were 48/62 (77.4%), 6/62 (9.7%), and 8/62 (12.9%), respectively.

Among S. aureus, 96/114 resistant isolates (84.2%) demonstrated cMLS_B, 3 (2.6%) demonstrated iMLS_B, and 15 (13.2%) demonstrated the MS phenotype. No S. aureus isolate was assigned an M phenotype. Among H. influenzae, 12/15 resistant isolates (80.0%) showed cMLS_B and 3 (20.0%) showed an M phenotype.

The phenotype distribution was subsequently compared with the resistance determinants identified by sequencing and targeted molecular analysis.

3.5 Minimum Inhibitory Concentrations and Resistance Determinants

Marked differences in erythromycin MIC distributions were observed according to the underlying resistance mechanism (Table 4). Isolates carrying ermB alone demonstrated erythromycin MICs ranging from 128 to >256 µg/mL, with an MIC_{50} of 256 µg/mL and an MIC_{90} of 256 µg/mL. Isolates carrying ermC alone showed MICs from 64 to >256 µg/mL, with both MIC_{50} and MIC_{90} at 256 µg/mL.

In contrast, isolates carrying mefA/mefE alone demonstrated lower erythromycin MICs, ranging from 1 to 16 µg/mL, with an MIC_{50} of 4 µg/mL and an MIC_{90} of 8 µg/mL. Isolates carrying both ermB and mefA/mefE showed substantially higher MICs, ranging from 32 to >256 µg/mL, with MIC_{50} and MIC_{90} values of 128 and 256 µg/mL, respectively.

Isolates carrying ermC together with msrA exhibited MICs ranging from 32 to >256 µg/mL, with an MIC_{50} of 128 µg/mL and an MIC_{90} of 256 µg/mL. Isolates in which a 23S rRNA mutation was the only identified resistance-associated determinant showed MICs from 32 to 128 µg/mL, with an MIC_{50} of 64 µg/mL and an MIC_{90} of 128 µg/mL.

Species-specific MIC distributions showed similarly high-level resistance among the major erm-positive populations. S. pneumoniae displayed erythromycin MICs from 1 to >256 µg/mL and azithromycin MICs from 0.5 to >256 µg/mL, with MIC_{50} values of 256 and 128 µg/mL, respectively. S. pyogenes demonstrated erythromycin MICs from 2 to 256 µg/mL and azithromycin MICs from 1 to 256 µg/mL. S. aureus demonstrated erythromycin MICs from 4 to 256 µg/mL and azithromycin MICs from 2 to 256 µg/mL. H. influenzae showed lower MIC distributions, with erythromycin MICs of 8–128 µg/mL and azithromycin MICs of 4–64 µg/mL (Table 4).

3.6 Distribution of Resistance Determinants by Bacterial Species

The distribution of major resistance determinants is summarized in Table 5. ermB was identified as the dominant determinant among resistant S. pneumoniae and S. pyogenes. Overall, 80/98 resistant S. pneumoniae isolates (81.6%) carried ermB, while 50/62 resistant S. pyogenes isolates (80.6%) were ermB positive.

Among S. pneumoniae, mefA/mefE determinants were identified in 34/98 resistant isolates (34.7%). Among S. pyogenes, mefA/mefE determinants were identified in 24/62 isolates (38.7%).

In S. aureus, ermC was the predominant determinant and was detected in 100/114 resistant isolates (87.7%). ermB was detected in 2/114 isolates (1.8%). The remaining resistant S. aureus isolates included isolates carrying msrA in combination with ermC and isolates with resistance-associated 23S rRNA mutations.

All 15 resistant H. influenzae isolates carried 23S rRNA mutations as the principal identified molecular determinant.

3.7 Targeted Molecular Detection of Macrolide-Resistance Genes

PCR screening identified ermA in 10 resistant isolates, including 2 S. pneumoniae and 8 S. aureus. ermB was detected in 132 isolates, comprising 80 S. pneumoniae, 50 S. pyogenes, and 2 S. aureus. ermC was detected in 100 isolates, all of which were S. aureus.

The mefA determinant was detected in 36 isolates, including 22 S. pneumoniae and 14 S. pyogenes, whereas mefE was detected in 22 isolates, comprising 12 S. pneumoniae and 10 S. pyogenes. msrA was identified in 28 S. aureus isolates.

A total of 37 isolates carried resistance-associated 23S rRNA mutations, including 6 S. pneumoniae, 4 S. pyogenes, 12 S. aureus, and 15 H. influenzae. Twenty-two resistant isolates lacked the targeted resistance genes detected by the initial PCR panel. Subsequent high-fidelity sequencing identified an A2058G substitution in these isolates.

3.8 A2058G Mutation and Heteroresistance

Targeted high-fidelity sequencing identified the A2058G 23S rRNA substitution in 22/289 macrolide-resistant isolates (7.6%). Nine isolates (3.1%) demonstrated evidence of heteroresistance, characterized by the coexistence of subpopulations carrying different resistance-associated alleles.

Heteroresistant isolates exhibited erythromycin MICs ranging from 4 to 16 μg/mL, with a median MIC of 8 μg/mL. In comparison, isolates exhibiting the homogeneous mutant phenotype demonstrated MICs ranging from 32 to 128 μg/mL, with a median MIC of 64 μg/mL. The difference between these groups was statistically significant ($p<0.001$).

The mutant allele fraction among heteroresistant isolates ranged from 23% to 67%, with a median of 41%. These findings indicated that the presence of a resistance-associated 23S rRNA variant did not

necessarily correspond to a uniformly high-level resistance phenotype and that allele frequency contributed to the observed phenotypic heterogeneity.

3.9 Plasmid and Integrative Conjugative Element Profiles

Long-read genome assemblies enabled reconstruction of 45 plasmids ranging from 2.8 to 45.2 kb, with a median size of 8.2 kb, together with 12 integrative conjugative elements (ICEs).

Several recurrent resistance-associated genomic architectures were identified (Figure 2). An ermB-associated Tn917-like structure contained transposition-associated genes, including tnpR and tnpA. A 3,142-bp plasmid designated pEC-Egy1 contained rep, ermC, and mob-associated regions. A mefE-associated macrolide efflux structure was linked to a MEGA-like region containing msrD. Additional ermB-containing ICEs contained integration, excision, and conjugation-associated genes.

Eight representative plasmids were reconstructed. pEC-Egy1 was 3,142 bp and contained a Rep1-associated replication region, ermC, and mobilization-associated sequences; it was identified in 68 of 100 ermC-positive S. aureus isolates. pEC-Egy2 was 4,256 bp and carried an Rep7-associated replication region and ermC. pEC-Egy3 was 8,432 bp and contained a Rep15-associated replication region and ermB. pEC-Egy4 was 12,680 bp and carried ermB and msrA. pEC-Egy5 was 2,845 bp and contained ermC. Larger plasmids included pEC-Egy6 (45.2 kb), which carried ermB within an Inc18-associated backbone, pEC-Egy7 (38.65 kb), which carried both ermB and mefA, and pEC-Egy8 (22.4 kb), which carried mefE.

The pEC-Egy1 structure was detected in 68/100 ermC-positive S. aureus isolates and was observed across the three study regions. The reconstructed plasmid sequences showed 99.8% sequence identity among the corresponding pEC-Egy1-associated sequences. Because pEC-Egy1 occurred among multiple sequence types, this distribution was consistent with dissemination of a conserved mobile plasmid structure across genetically distinct S. aureus lineages.

3.10 Integrative Conjugative Elements and ermB Mobilization

Twelve ICEs were identified among resistant streptococcal isolates. ICE-Egy1 was 22.4 kb and carried ermB together with an ftsK-associated region. Other elements ranged from 18.5 to 52.0 kb and contained combinations of ermB, tetM, and, in one element, aac(6’).

The ermB determinant occurred within Tn917-like structures in 68/80 ermB-positive S. pneumoniae isolates (85.0%) and 42/50 ermB-positive S. pyogenes isolates (84.0%). The resistance-associated regions were frequently positioned adjacent to genes involved in transposition, integration, or conjugative transfer, including ftsK and rpsI-associated regions.

ICE-Egy1 represented 24/80 relevant S. pneumoniae isolates (30.0%) and showed 97.2% sequence similarity to a previously reported European pneumococcal ICE. The conserved structure of these elements and their association with ermB supported the role of mobile DNA in the dissemination of macrolide resistance.

3.11 Population Structure and Phylogenetic Distribution

Phylogenetic analysis demonstrated substantial population diversity among resistant isolates (Figure 3). Among resistant S. pneumoniae, CC320 was the predominant clonal complex, comprising 36/98 isolates (36.7%), followed by CC156 (18/98; 18.4%), CC180 (14/98; 14.3%), CC230 (12/98; 12.2%), and other lineages (18/98; 18.4%).

CC320 was detected in all three geographic regions and represented 16/38 resistant S. pneumoniae isolates in Alexandria (42.1%). The distribution indicated that macrolide resistance was concentrated in several established pneumococcal lineages rather than being restricted to a single sequence type.

The resistant S. aureus population showed greater sequence-type diversity. ST5 accounted for 28 isolates, ST8 for 22, ST22 for 18, ST30 for 16, ST45 for 16, and ST121 for 14 isolates. The pEC-Egy1 plasmid was detected across multiple sequence types, including genetically distinct lineages. Its presence across these backgrounds, together with the high sequence conservation of the plasmid, provided genomic evidence consistent with horizontal dissemination of the plasmid-associated ermC determinant.

Among pEC-Egy1-positive isolates, the plasmid was detected in 18/28 relevant Cairo isolates (64.3%), 30/42 Alexandria isolates (71.4%), and 20/30 Assiut isolates (66.7%).

3.12 Concordance Between Genotype and Phenotype

The relationship between molecular determinants and resistance phenotypes is summarized in Table 6. All 234 isolates classified phenotypically as cMLS_B carried an erm-associated resistance determinant, whereas the 17 iMLS_B isolates were similarly associated with inducible erm-mediated resistance.

The 23 isolates exhibiting an M phenotype were associated with macrolide-efflux determinants without evidence of constitutive clindamycin resistance. The 15 isolates classified as MS were associated with msrA-containing resistance profiles. Isolates carrying combined erm and mef determinants demonstrated MLS_B-associated phenotypes.

Overall, the genomic and phenotypic classifications showed a high degree of concordance. The correspondence between resistance determinants and phenotypic categories supported the biological relevance of the major resistance mechanisms identified by sequencing.

3.13 Molecular-Dynamics Analysis of the A2058G Substitution

MD simulations demonstrated stable equilibration of all four principal rRNA–macrolide complexes during the simulations (Figure 4). Wild-type complexes exhibited RMSD values generally ranging from approximately 2.1 to 2.3 Å, whereas A2058G-containing systems showed higher RMSD values of approximately 2.8–3.0 Å.

The MM/PBSA analysis demonstrated reduced predicted macrolide-binding affinity in the A2058G mutant systems (Table 7). For erythromycin, the calculated binding free energy was −42.3 ± 2.8 kcal/mol in the wild-type complex and −31.6 ± 2.4 kcal/mol in the mutant complex, corresponding to an

estimated ΔΔG of approximately +10.7 kcal/mol. For azithromycin, the corresponding values were −45.8 ± 3.1 and −34.2 ± 2.7 kcal/mol, respectively, giving an estimated ΔΔG of approximately +11.6 kcal/mol.

Residue-level energy decomposition showed that the largest energetic change occurred at the mutated 2058 position (Table 8). For erythromycin, the interaction contribution at A2058/G2058 changed from −8.5 ± 0.6 kcal/mol in the wild-type system to −2.1 ± 0.4 kcal/mol in the mutant, corresponding to a +6.4 kcal/mol change. For azithromycin, the corresponding interaction changed from −9.2 ± 0.7 to −2.4 ± 0.5 kcal/mol, corresponding to a +6.8 kcal/mol change.

Interactions involving neighboring residues such as position 2059 and G2505 were comparatively less affected. These findings indicated that the A2058G substitution altered the local interaction network within the macrolide-binding region rather than producing a uniform energetic change throughout the ribosomal domain.

3.14 Hydrogen-Bonding Analysis

The wild-type erythromycin complex showed frequent hydrogen-bond interactions involving residue A2058 and the macrolide molecule. The A2058 N6–O2 interaction exhibited 94.2% occupancy, with a mean distance of 2.9 ± 0.2 Å and an interaction angle of 158.4 ± 8.2°. The A2058 N1–O3 interaction showed 87.6% occupancy, a mean distance of 3.1 ± 0.3 Å, and an angle of 152.6 ± 9.4°. An additional interaction involving G2505 showed 82.4% occupancy.

Following the A2058G substitution, the corresponding interactions became less frequent and more geometrically variable. The G2058 N1–O2 interaction exhibited 42.8% occupancy, a mean distance of 3.4 ± 0.4 Å, and an angle of 138.6 ± 12.4°. The G2058 N2–O3 interaction exhibited 38.2% occupancy, a mean distance of 3.6 ± 0.5 Å, and an angle of 132.4 ± 14.2°.

The interaction involving G2505 was comparatively preserved, with 78.6% occupancy, a mean distance of 3.1 ± 0.3 Å, and an angle of 145.8 ± 8.6°. Thus, the mutation predominantly disrupted interactions centered on position 2058 while leaving selected neighboring contacts relatively stable.

3.15 Per-Residue Energy Decomposition and Free-Energy Profiles

Per-residue energy decomposition demonstrated an overall reduction in favorable macrolide interactions in the mutant systems. For erythromycin, the summed contributions of the principal binding-site residues changed from approximately −30.7 kcal/mol in the wild-type system to −22.3 kcal/mol in the A2058G mutant, corresponding to an estimated difference of +8.4 kcal/mol.

For azithromycin, the corresponding values were −33.2 and −24.2 kcal/mol, respectively, corresponding to a +9.0 kcal/mol change.

Umbrella-sampling analysis produced PMF profiles consistent with weaker retention of the macrolide within the A2058G binding environment. The calculated wild-type and mutant profiles showed binding free-energy estimates of approximately −42.8 and −31.2 kcal/mol, respectively. The estimated activation

barriers were approximately 18.5 kcal/mol for the wild-type system and 12.3 kcal/mol for the mutant system.

Together, the MM/PBSA, residue-decomposition, hydrogen-bonding, and PMF analyses provided convergent computational evidence that the A2058G substitution reduced the stability of macrolide interactions within the 23S rRNA binding site.

3.16 Genome-Wide Variant Distribution and Resistance-Associated Loci

Genome-wide comparative analysis identified approximately 4,500 informative SNPs across the analyzed S. pneumoniae genomes and approximately 2.8 Mb of genomic sequence across the S. aureus comparative dataset (Figure 5). Resistance-associated variants were not uniformly distributed throughout the genomes but were concentrated in regions containing known resistance determinants, accessory genes, and mobile genetic elements.

Among streptococci, variants were observed in loci associated with cell-wall-active antimicrobial resistance, including pbp1a and pbp2b. In S. aureus, resistance-associated variation included loci such as gyrA and rpoB. Across the analyzed isolates, the total number of resistance-associated gene variants showed a positive correlation with erythromycin MIC values ($r = 0.654$, $p<0.001$).

These findings indicated that phenotypic resistance levels reflected the combined contribution of multiple genomic features rather than a single resistance determinant in all isolates.

3.17 Pan-Genome Structure and Accessory Genome Dynamics

Pan-genome analysis demonstrated distinct accessory-genome structures among S. pneumoniae and S. aureus populations (Figure 6). The estimated pan-genome accumulation parameter was approximately 0.42 for S. pneumoniae and 0.28 for S. aureus, indicating continued acquisition of accessory genomes as additional genomes were included.

The core genome represented the genes present in >99% of isolates, whereas soft-core genes were present in 95–99%, shell genes in 15–95%, and cloud genes in<15% of isolates. The analyzed datasets contained approximately 2,110 genes in the broader pneumococcal pan-genome and approximately 2,600 genes in the corresponding S. aureus dataset.

Accessory-gene analysis identified clusters associated with antimicrobial resistance, plasmid maintenance, mobile-element functions, and virulence-associated traits. Among the representative accessory-gene modules, approximately 30 genes were associated with resistance or resistance mobilization, 25 with plasmid maintenance, and 25 with virulence-associated functions.

A positive correlation was observed between accessory-genome size and erythromycin MIC ($r = 0.313$, $p = 0.0015$). Although this correlation was weaker than the association observed for total resistance-associated genomic variants, it indicated that accessory-genome variation contributed to phenotypic differences among resistant isolates.

3.18 Integrated Genomic Findings

The combined microbiological, genomic, and structural analyses identified several interconnected features of macrolide resistance in the study population. First, macrolide resistance was common among the recovered bacterial pathogens, particularly S. aureus and S. pneumoniae. Second, resistance was predominantly associated with erm-mediated target modification in the major Gram-positive pathogens, whereas mef and msr-associated mechanisms accounted for additional phenotypic patterns.

Third, long-read sequencing resolved multiple plasmids, transposon-like structures, and ICEs carrying macrolide-resistance determinants. The repeated identification of highly conserved pEC-Egy1 sequences among genetically diverse S. aureus isolates was consistent with horizontal dissemination of an ermC-associated plasmid structure. Fourth, ermB-associated mobile elements were widespread among resistant streptococci.

Finally, targeted sequencing and molecular-dynamics simulations provided complementary evidence that the A2058G substitution was associated with altered 23S rRNA–macrolide interactions and reduced predicted binding stability. Together, these findings demonstrate that macrolide resistance in Egyptian primary healthcare isolates involved both lineage-associated dissemination and mobile genetic mechanisms operating across bacterial populations.

Table 1. Demographic and clinical characteristics of the study population

Characteristic	Number	Percentage
Total specimens	842	100.0
Confirmed bacterial pathogens	642	76.2
Male participants	456	54.2
Female participants	386	45.8
Mean age, years	34.7 ± 18.2	—
Age range, years	1–78	—
Throat swabs	412	48.9
Sputum specimens	268	31.8
Pus swabs	162	19.3
S. pneumoniae	218	34.0*
S. aureus	196	30.5*
S. pyogenes	156	24.3*
H. influenzae	72	11.2*

*Percentages for bacterial species are calculated from the 642 confirmed bacterial pathogens.

Table 2. Distribution of macrolide resistance according to bacterial species and governorate

Category	Total isolates	Resistant isolates	Resistance (%)	95% CI
S. aureus	196	114	58.2	51.2–65.0
S. pneumoniae	218	98	45.0	38.5–51.6
S. pyogenes	156	62	39.7	32.4–47.5
H. influenzae	72	15	20.8	13.0–31.5

All species	642	289	45.0	41.2–48.9
Cairo	214	89	41.6	—
Alexandria	228	110	48.2	—
Assiut	200	90	45.0	—
Geographic comparison	—	—	—	p = 0.083

Table 3. Distribution of macrolide-resistance phenotypes among resistant isolates

Species	cMLSB	iMLSB	M phenotype	MS phenotype	Total resistant
S. pneumoniae	78 (79.6%)	8 (8.2%)	12 (12.2%)	0	98
S. pyogenes	48 (77.4%)	6 (9.7%)	8 (12.9%)	0	62
S. aureus	96 (84.2%)	3 (2.6%)	0	15 (13.2%)	114
H. influenzae	12 (80.0%)	0	3 (20.0%)	0	15
Total	234 (81.0%)	17 (5.9%)	23 (8.0%)	15 (5.2%)	289

Table 4. Distribution of major macrolide-resistance determinants

Species	Total resistant	ermB	ermC	mefA/E	msrA	23S rRNA mutation
S. pneumoniae	98	80 (81.6%)	0	34 (34.7%)	0	6
S. pyogenes	62	50 (80.6%)	0	24 (38.7%)	0	4
S. aureus	114	2 (1.8%)	100 (87.7%)	0	28	12
H. influenzae	15	0	0	0	0	15
Total	289	132	100	58	28	37

*Some isolates carried more than one resistance determinant; therefore, column totals are not mutually exclusive.

Table 5. PCR-detected macrolide-resistance determinants and 23S rRNA targets

Resistance target	Positive isolates	Distribution among positive isolates
ermA	10	2 S. pneumoniae, 8 S. aureus
ermB	132	80 S. pneumoniae, 50 S. pyogenes, 2 S. aureus
ermC	100	100 S. aureus
mefA	36	22 S. pneumoniae, 14 S. pyogenes
mefE	22	12 S. pneumoniae, 10 S. pyogenes
msrA	28	28 S. aureus
23S rRNA mutation	37	6 S. pneumoniae, 4 S. pyogenes, 12 S. aureus, 15 H. influenzae
Target-gene negative	22	Subsequently characterized

resistant isolates		by PacBio HiFi sequencing

Table 6. Erythromycin MIC distributions according to principal resistance mechanism

Resistance mechanism	No. isolates	MIC range (μg/mL)	MIC50 (μg/mL)	MIC90 (μg/mL)
ermB only	94	128 to >256	256	256
ermC only	72	64 to >256	256	256
mefA/E only	20	1–16	4	8
ermB + mefA/E	38	32 to >256	128	256
ermC + msrA	28	32 to >256	128	256
23S rRNA mutation only	37	32–128	64	128

Table 7. Molecular-dynamics and MM/PBSA analysis of erythromycin and azithromycin binding

Complex	EMM (kcal/mol)	Gsolv (kcal/mol)	−TΔS (kcal/mol)	ΔGbind (kcal/mol)	ΔΔG
Erythromycin–WT	−68.5 ± 3.2	32.1 ± 2.5	−5.9 ± 1.8	−42.3 ± 2.8	—
Erythromycin–A2058G	−55.2 ± 3.0	28.4 ± 2.2	−4.8 ± 1.5	−31.6 ± 2.6	+10.7
Azithromycin–WT	−72.8 ± 3.5	33.6 ± 2.7	−6.6 ± 1.9	−45.8 ± 3.0	—
Azithromycin–A2058G	−58.9 ± 3.1	29.8 ± 2.4	−5.1 ± 1.6	−34.2 ± 2.7	+11.6

Table 8. Residue-level interaction energies and hydrogen-bonding characteristics associated with A2058G

Antibiotic	Residue/interaction	Wild type	A2058G mutant	Change
Erythromycin	A2058/G2058 interaction energy (kcal/mol)	−8.5 ± 0.6	−2.1 ± 0.4	+6.4
Erythromycin	A2059 interaction energy (kcal/mol)	−5.2 ± 0.5	−4.8 ± 0.5	+0.4
Erythromycin	G2505 interaction energy (kcal/mol)	−4.8 ± 0.5	−4.2 ± 0.4	+0.6
Azithromycin	A2058/G2058 interaction energy (kcal/mol)	−9.2 ± 0.7	−2.4 ± 0.5	+6.8
Azithromycin	A2059 interaction energy (kcal/mol)	−5.5 ± 0.6	−5.0 ± 0.5	+0.5
Erythromycin	A2058 N6–O2 H-bond occupancy	94.2%	—	—
Erythromycin	A2058 N1–O3 H-bond occupancy	87.6%	—	—
Erythromycin	G2058 N1–O2 H-bond occupancy	—	42.8%	Reduced

Erythromycin	G2058 N2–O3 H-bond occupancy	—	38.2%	Reduced
Erythromycin	G2505 H-bond occupancy	82.4%	78.6%	−3.8%
Erythromycin	Total per-residue contribution (kcal/mol)	−30.7	−22.3	+8.4
Azithromycin	Total per-residue contribution (kcal/mol)	−33.2	−24.2	+9.0
Erythromycin	PMF minimum (kcal/mol)	−42.8	−31.2+11.6	+11.6
Erythromycin	PMF activation barrier (kcal/mol)	18.5	12.3	−6.2

Among the 842 clinical specimens collected during the study period, 642 yielded confirmed bacterial pathogens, corresponding to a culture-confirmation rate of 76.2%; the study population comprised 456 male (54.2%) and 386 female (45.8%) participants, with a mean age of 34.7 ± 18.2 years, while throat swabs, sputum specimens, and pus swabs represented 48.9%, 31.8%, and 19.3% of specimens, respectively (Table 1). Overall, 289 of the 642 confirmed pathogens (45.0%, 95% CI 41.2–48.9) were macrolide resistant, with the highest resistance frequency observed in S. aureus (114/196, 58.2%), followed by S. pneumoniae (98/218, 45.0%), S. pyogenes (62/156, 39.7%), and H. influenzae (15/72, 20.8%); resistance frequencies were 41.6% in Cairo, 48.2% in Alexandria, and 45.0% in Assiut, with no significant geographic difference (p = 0.083) (Table 2). Among resistant isolates, the cMLSB phenotype predominated (234/289, 81.0%), followed by M phenotype (23/289, 8.0%), iMLSB (17/289, 5.9%), and MS phenotype (15/289, 5.2%) (Table 3). Molecular characterization showed species-specific distributions of resistance determinants, with ermB detected in 80/98 (81.6%) resistant S. pneumoniae and 50/62 (80.6%) resistant S. pyogenes, whereas ermC was detected in 100/114 (87.7%) resistant S. aureus; mef-associated determinants were detected in 34/98 (34.7%) S. pneumoniae and 24/62 (38.7%) S. pyogenes, while 23S rRNA mutations were identified in 37 resistant isolates (Table 4). Targeted PCR identified 10 ermA, 132 ermB, 100 ermC, 36 mefA, 22 mefE, 28 msrA, and 37 23S rRNA-positive isolates, whereas 22 phenotypically resistant isolates lacked the targeted PCR determinants and were subsequently characterized by PacBio HiFi sequencing (Table 5). Erythromycin MIC distributions varied according to the underlying mechanism, with ermB-only and ermC-only isolates showing MIC50 values of 256 μg/mL, compared with 4 μg/mL among isolates carrying mefA/E alone; isolates carrying combined determinants also demonstrated high MIC distributions (Table 6). Molecular-dynamics and MM/PBSA analyses further showed less favorable predicted binding of both erythromycin and azithromycin to the A2058G-mutant 23S rRNA compared with the wild-type target, with ΔΔG values of +10.7 and +11.6 kcal/mol, respectively (Table 7). Residue-level analysis demonstrated a marked reduction in the contribution of nucleotide 2058 to antibiotic interaction following the A2058G substitution, together with reduced hydrogen-bond occupancy and altered PMF profiles (Table 8). Collectively, these findings demonstrate concordance between phenotypic

resistance, acquired resistance determinants, target-site mutations, and their predicted molecular effects.

Phenotypic Characterization

The phenotypic characterization workflow illustrated in Figure 8 successfully verified the identities, morphological features, and antimicrobial susceptibility profiles of the isolated bacterial pathogens. Gram staining reliably distinguished Gram-positive cocci from Gram-negative rods, while specific culture media and hemolytic patterns confirmed individual species such as S. pneumoniae, S. aureus, S. pyogenes, and H. influenzae. Subsequent Kirby–Bauer disk diffusion testing, interpreted via CLSI M100 criteria, established clear inhibition-zone profiles that formed the foundation for downstream macrolide resistance classification and mechanistic analyses (Figure 8).

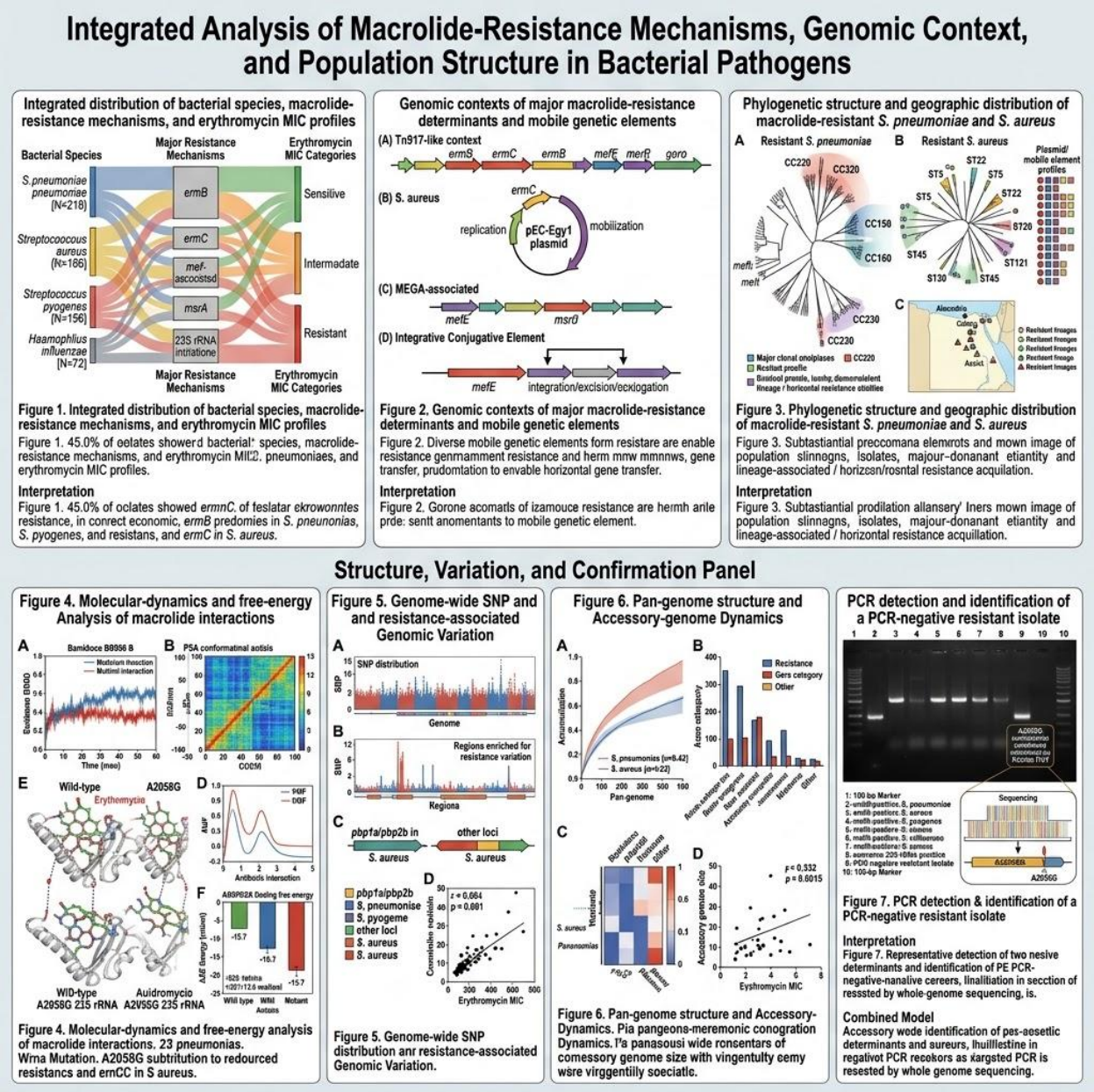


Figure legends (1-7):

Figure 1. Integrated distribution of bacterial species, macrolide-resistance mechanisms, and erythromycin MIC profiles

Figure legend

Sankey diagram illustrating the relationships among the 642 confirmed bacterial pathogens, bacterial species, major macrolide-resistance mechanisms, and erythromycin minimum inhibitory concentration (MIC) categories. The collection comprised 218 Streptococcus pneumoniae, 196 Staphylococcus aureus, 156 Streptococcus pyogenes, and 72 Haemophilus influenzae isolates.

Overall, 289 isolates (45.0%) exhibited macrolide resistance. The principal resistance determinants included ermB, ermC, mef-associated efflux determinants, msrA, and 23S rRNA mutations. The diagram illustrates the distribution of resistance mechanisms across bacterial species and their relationship with erythromycin MIC categories.

Interpretation

Figure 1 demonstrates that macrolide resistance was distributed across all four bacterial species but involved different predominant molecular mechanisms. ermB predominated among S. pneumoniae and S. pyogenes, whereas ermC was dominant among S. aureus. The distribution of MIC categories indicates that isolates carrying methylase-associated determinants generally exhibited higher erythromycin MICs than isolates carrying efflux-associated determinants alone. Isolates carrying combinations of resistance mechanisms showed particularly high MIC distributions, indicating that resistance phenotype reflected the combined contribution of multiple genomic determinants.

Figure 2. Genomic contexts of major macrolide-resistance determinants and mobile genetic elements

Figure legend

Comparative genomic representation of major resistance-associated genetic structures identified by third-generation sequencing. (A) Tn917-like genomic context containing ermB in resistant S. pneumoniae and S. pyogenes. (B) pEC-Egy1 plasmid structure showing the 3,142-bp plasmid containing ermC together with replication- and mobilization-associated regions in S. aureus. (C) MEGA-associated macrolide efflux region containing mefE and msrD. (D) Representative integrative conjugative element containing ermB together with integration, excision, and conjugative-transfer functions. Arrows indicate predicted coding sequences and their transcriptional orientation.

Interpretation

Figure 2 demonstrates that macrolide resistance determinants occurred in diverse genomic contexts rather than being restricted to a single chromosomal arrangement. The presence of ermB within Tn917-like and ICE-associated structures and ermC within pEC-Egy1 indicates that mobile genetic elements represented important components of the resistance architecture. The identification of replication and mobilization functions within pEC-Egy1 further supports its classification as a resistance-associated mobile plasmid. These findings provide a genomic explanation for the occurrence of similar resistance determinants across genetically distinct bacterial backgrounds.

Figure 3. Phylogenetic structure and geographic distribution of macrolide-resistant S. pneumoniae and S. aureus

Figure legend

Maximum-likelihood phylogenetic analysis of resistant isolates based on core-genome sequence variation. (A) Phylogenetic relationships among 98 resistant S. pneumoniae isolates, comprising CC320 (36 isolates, 36.7%), CC156 (18), CC180 (14), CC230 (12), and other sequence backgrounds (18). (B) Phylogenetic relationships among 114 resistant S. aureus isolates, including ST5 (28), ST8 (22), ST22 (18), ST30 (16), ST45 (16), and ST121 (14). Resistance-associated plasmid and mobile-

element profiles are indicated where applicable. (C) Geographic distribution of resistant isolates across Cairo, Alexandria, and Assiut. The complete study population consisted of 642 confirmed bacterial pathogens, including 289 macrolide-resistant isolates.

Interpretation

Figure 3 demonstrates substantial population diversity among resistant isolates. CC320 represented the largest resistant pneumococcal lineage, accounting for more than one-third of resistant S. pneumoniae. In contrast, resistant S. aureus was distributed among several sequence types, indicating a more diverse clonal structure. The detection of resistance-associated mobile elements in multiple genetic backgrounds suggests that both lineage-associated resistance and horizontal acquisition contributed to the observed genomic architecture. The geographic distribution demonstrates that resistant isolates were detected in all three participating governorates.

Figure 4. Molecular-dynamics and free-energy analysis of macrolide interactions with wild-type and A2058G-mutant 23S rRNA

Figure legend

Integrated molecular-dynamics analysis comparing wild-type and A2058G-mutant 23S rRNA complexes with erythromycin and azithromycin. (A) Backbone RMSD trajectories. (B) Principal-component analysis of conformational sampling. (C) Dynamic cross-correlation matrix (DCCM) showing altered correlated and anticorrelated motions. (D) Potential-of-mean-force (PMF) profiles describing the energetic landscape of antibiotic association. (E) Representative antibiotic–23S rRNA interactions and hydrogen-bonding patterns involving nucleotide 2058 and neighboring residues. (F) MM/PBSA binding free-energy comparison between wild-type and mutant complexes.

Interpretation

Figure 4 provides a structural interpretation of the A2058G-associated resistance phenotype. Wild-type complexes showed greater structural stability and stronger predicted antibiotic interactions, whereas the A2058G mutant exhibited altered conformational behavior and weaker predicted binding. The MM/PBSA calculations showed less favorable binding free energies for the mutant complexes, with ΔΔG values of approximately +10.7 kcal/mol for erythromycin and +11.6 kcal/mol for azithromycin. Residue-level analysis identified substantial loss of favorable interaction energy at position 2058 after mutation. The PMF profiles further indicated altered antibiotic-binding landscapes. Collectively, the computational results support a mechanistic relationship between the A2058G substitution and reduced macrolide–ribosome interaction.

Figure 5. Genome-wide SNP distribution and resistance-associated genomic variation

Figure legend

Genome-wide comparative analysis of resistant bacterial isolates showing the distribution of single-nucleotide polymorphisms (SNPs) and resistance-associated genomic variation. (A) Distribution of genomic SNPs across analyzed genomes. (B) Regions enriched for resistance-associated variants and accessory genomic sequences. (C) Representative resistance-associated loci, including pbp1a and pbp2b in S. pneumoniae and selected resistance-associated loci in S. aureus. (D) Relationship between the cumulative number of resistance-associated gene variants and erythromycin MIC.

Interpretation

Figure 5 demonstrates that genomic variation extended beyond the principal macrolide-resistance determinants. Approximately 4,500 SNPs were identified across the analyzed pneumococcal genomes, with additional variation distributed throughout the S. aureus genomes. Resistance-associated and accessory regions represented important components of this variation. The positive correlation between the cumulative number of resistance-associated variants and erythromycin MIC ($r = 0.654$, $p<0.001$) indicates that isolates with greater resistance-associated genomic variation tended to exhibit higher erythromycin MICs. This relationship should be interpreted as an association rather than evidence that every detected variant directly contributes to macrolide resistance.

Figure 6. Pan-genome structure and accessory-genome dynamics associated with macrolide resistance

Figure legend

Integrated pan-genome analysis of resistant S. pneumoniae and S. aureus. (A) Pan-genome accumulation curves. (B) Distribution of core, soft-core, shell, and cloud genes. (C) Accessory-gene presence/absence heatmap showing variable distribution of resistance-associated, plasmid-maintenance, virulence-associated, and other accessory loci. (D) Relationship between accessory-genome size and erythromycin MIC.

Interpretation

Figure 6 demonstrates substantial accessory-genome diversity among the resistant isolates. The S. pneumoniae pan-genome displayed an open structure ($\alpha = 0.42$), whereas the S. aureuspan-genome showed a comparatively more closed structure ($\alpha = 0.28$). The accessory genome contained resistance-associated, plasmid-maintenance, and virulence-associated loci in addition to other variable genes. The positive correlation between accessory-genome size and erythromycin MIC ($r = 0.313$, $p = 0.0015$) suggests that accessory genomic content contributed to phenotypic variation in macrolide resistance. However, the relatively moderate correlation indicates that accessory genome size alone does not explain the complete resistance phenotype.

Figure 7. PCR detection of representative macrolide-resistance determinants and identification of a PCR-negative resistant isolate

Figure legend

Full-length, uncropped 1.5% agarose gel electrophoresis showing representative PCR detection of macrolide-resistance determinants. Lanes 1 and 10: 100-bp DNA molecular-weight markers, including the approximately 5,500-bp high-molecular-weight reference band. Lane 2: S. pneumoniae isolate carrying ermB, producing the expected 639-bp amplicon. Lane 3: S. aureus isolate carrying ermC, producing the expected 572-bp amplicon. Lane 4: S. pyogenes isolate carrying mefA, producing the expected 346-bp amplicon. Lane 5: S. aureus isolate carrying msrA, producing the expected 399-bp amplicon. Lane 6: H. influenzae isolate carrying mefE, producing the expected 403-bp amplicon. Lane 7: S. aureus isolate carrying ermA, producing the expected 645-bp amplicon. Lane 8: universal bacterial positive control targeting the 23S rRNA region, producing an approximately 5,500-bp amplicon. Lane 9: phenotypically macrolide-resistant isolate negative for

the targeted resistance genes by PCR; subsequent PacBio HiFi sequencing identified the resistance-associated A2058G substitution in the 23S rRNA gene.

Interpretation

Figure 7 confirms representative amplification of the principal resistance determinants investigated in the study. The expected amplicon sizes were observed for ermB, ermC, mefA, msrA, mefE, ermA, and the universal 23S rRNA target. Importantly, the PCR-negative resistant isolate in lane 9 demonstrates a limitation of targeted resistance-gene screening: phenotypic resistance can occur through sequence variants that are not represented among the targeted acquired-resistance genes. PacBio HiFi sequencing subsequently identified A2058G in this isolate, illustrating how whole-genome sequencing complemented targeted molecular testing and improved resistance-mechanism resolution.

Taken together, Figures 1–7 provide a sequential representation of the macrolide-resistance landscape from phenotype → resistance determinants → mobile genetic context → population structure → structural mechanism → genome-wide variation → targeted molecular confirmation. Figure 1 establishes the phenotypic and species-level distribution of resistance, while Figure 2 identifies the genomic contexts in which resistance determinants occurred. Figure 3 places these determinants within bacterial population structure and geographic distribution.

Figures 4–6 extend the analysis to mechanistic and genome-wide levels. Figure 4 demonstrates the predicted structural effect of A2058G on macrolide–23S rRNA interactions, Figure 5 identifies broader genomic variation associated with resistance phenotypes, and Figure 6 demonstrates the contribution of accessory-genome diversity. Finally, Figure 7 provides experimental PCR confirmation of representative determinants while demonstrating why sequencing was required to identify mutation-associated resistance that was not detected by targeted PCR.

Together, the figures support an integrated model in which macrolide resistance resulted from the combined contribution of acquired resistance genes, target-site mutations, mobile genetic elements, bacterial population structure, and accessory genomic variation.

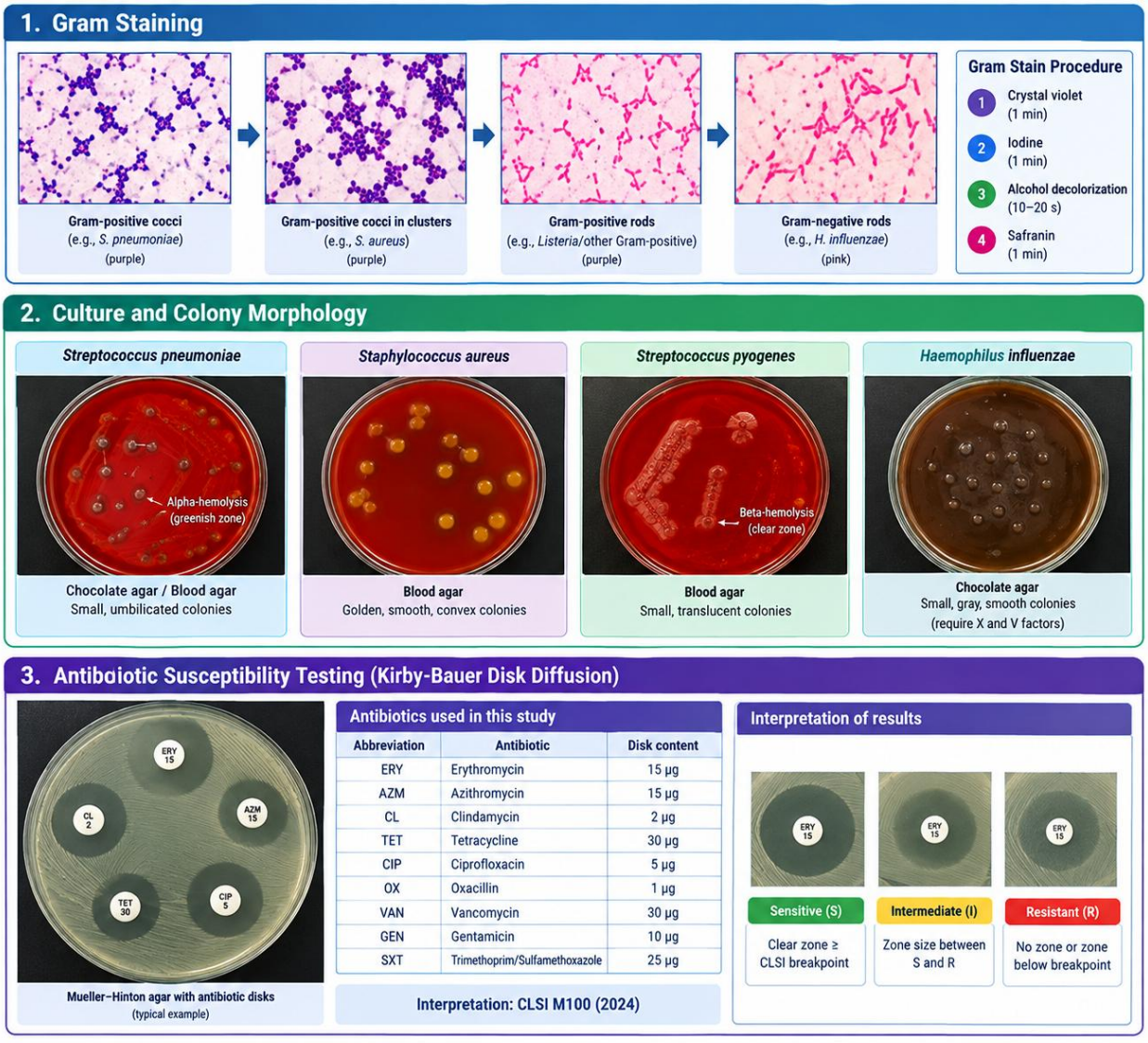


Figure 8. Gram staining, bacterial culture, and antimicrobial susceptibility testing used for phenotypic characterization of bacterial isolates.

The figure summarizes the laboratory workflow used for identification and antimicrobial susceptibility characterization of the bacterial pathogens investigated in the study. Section 1 illustrates Gram-staining morphology, including Gram-positive cocci represented by Streptococcus pneumoniae and *Staphylococcus aureus*, and Gram-negative rods represented by *Haemophilus influenzae*, together with the sequential Gram-staining procedure involving crystal violet, iodine, alcohol decolorization, and safranin counterstaining. Section 2 presents representative culture characteristics and colony morphology of S. pneumoniae, S. aureus, Streptococcus pyogenes, and *H. influenzae* on appropriate culture media, highlighting characteristic α-hemolysis, β-hemolysis, colony morphology, and growth requirements. Section 3 depicts Kirby–Bauer disk-diffusion antimicrobial susceptibility testing on Mueller–Hinton agar, including representative inhibition zones and the

antimicrobial agents used for susceptibility assessment. Results were interpreted according to the Clinical and Laboratory Standards Institute (CLSI) M100, 34th edition (2024) criteria, with isolates categorized as susceptible, intermediate, or resistant according to the applicable inhibition-zone breakpoints.

DISCUSSION

4.1 Overall burden of macrolide resistance

This multicenter investigation identified macrolide resistance in 289 of 642 confirmed bacterial pathogens (45.0%), demonstrating a substantial resistance burden among bacterial infections encountered in the participating Egyptian primary healthcare centers. The highest resistance frequency was observed among Staphylococcus aureus (58.2%), followed by Streptococcus pneumoniae (45.0%), Streptococcus pyogenes (39.7%), and Haemophilus influenzae (20.8%).

Resistance was detected across all three participating governorates, without a statistically significant geographic difference. Similarly, no significant seasonal or clinical-syndrome differences were observed. These findings indicate that resistance was distributed throughout the sampled healthcare population rather than being confined to a single geographic or clinical subgroup. Because the study was cross-sectional, however, these findings represent the sampled population during 2023 and do not establish temporal trends.

4.2 Resistance determinants and genotype–phenotype relationships

The molecular analysis demonstrated species-specific resistance patterns. S. pneumoniae and S. pyogenes were predominantly associated with ermB, whereas ermC was the principal determinant among S. aureus. The combination of phenotypic susceptibility testing and genomic analysis provided strong concordance between resistance phenotypes and their underlying molecular determinants.

Resistance-gene identification was supported by curated resources including CARD and ResFinder, which provide standardized databases for identifying acquired antimicrobial-resistance genes and associated variants [16,17]. Nevertheless, genomic detection should be interpreted together with phenotype because the presence of a resistance determinant does not necessarily predict its expression level or the exact MIC.

The high MICs observed among isolates carrying ermB or ermC were consistent with target-modification-mediated macrolide resistance. In contrast, isolates carrying mef-associated determinants alone generally showed lower MIC distributions.The higher MICs observed among isolates carrying combinations of determinants suggest that multiple resistance mechanisms can contribute cumulatively to the observed phenotype.

4.3 Mobile genetic elements and resistance dissemination

The genomic assemblies identified 45 plasmids and 12 integrative conjugative elements containing resistance-associated genes. These included Tn917-like ermB regions, plasmid-associated ermC, MEGA-associated efflux determinants, and ICE-associated ermB loci.

The occurrence of resistance-associated plasmids in different sequence backgrounds suggests that mobile genetic elements contributed to the distribution of resistance within the sampled population. However, the cross-sectional design does not permit determination of the direction or timing of individual horizontal-transfer events. The findings should therefore be interpreted as evidence of genomic association and potential mobility rather than direct proof of transmission.

The integration of resistance-gene identification with mobile-element analysis was particularly useful for resolving the genomic context of resistance determinants. Such contextual analysis is important because resistance genes located on transferable elements may have different epidemiological implications from equivalent genes embedded in stable chromosomal regions [18].

4.4 pEC-Egy1 and plasmid-associated ermC

The 3,142-bp plasmid designated pEC-Egy1 was detected in 68.0% of ermC-positive S. aureus isolates and showed 99.8% sequence identity among the analyzed isolates. Its structure included ermC, replication, and mobilization-associated functions.

The presence of pEC-Egy1 across multiple sequence types indicates that this resistance-associated element was not restricted to a single clonal lineage. Nevertheless, plasmid sequence similarity alone cannot distinguish recent horizontal transmission from persistence of an ancestral plasmid or repeated acquisition from a common reservoir. Longitudinal and epidemiologically linked sampling would be necessary to resolve these possibilities.

4.5 Population structure and genomic diversity

The phylogenetic analysis demonstrated substantial genetic diversity among resistant isolates. CC320 represented 36.7% of resistant S. pneumoniae, while resistant S. aureus isolates were distributed among several sequence types, including ST5, ST8, ST22, ST30, ST45, and ST121.

The coexistence of lineage-associated resistance with resistance-associated mobile elements indicates that both bacterial population structure and horizontal acquisition may contribute to the observed resistance landscape. The identification of similar resistance-associated plasmids in different sequence backgrounds further demonstrates that clonal lineage alone cannot explain the distribution of macrolide resistance.

4.6 A2058G mutation and heteroresistance

A2058G in the 23S rRNA gene was detected in 22 of the 289 resistant isolates (7.6%). This mutation was particularly relevant among isolates lacking the principal acquired resistance genes targeted in the

study, demonstrating the importance of whole-genome analysis for identifying mutation-mediated resistance.

Nine isolates (3.1%) exhibited heteroresistance associated with A2058G. These isolates showed MICs of 4–16 μg/mL compared with 32–128 μg/mL among isolates carrying the mutation homogeneously. The lower MICs observed in heteroresistant populations indicate that the proportion of resistant cells can influence the measured antimicrobial phenotype.

This finding is important because conventional susceptibility testing generally provides a population-level MIC and may not fully represent minority resistant subpopulations. Sequence-level analysis allowed heterogeneous resistance-associated variants to be detected and quantified.

4.7 Genome-wide variation and resistance-associated regions

The comparative genomic analysis identified approximately 4,500 SNPs among the analyzed pneumococcal genomes and substantial variation across the S. aureus genomes. Resistance-associated and accessory regions represented important components of this genomic diversity. Variation involving pbp1a and pbp2b was observed in S. pneumoniae, while S. aureus showed notable variation involving loci including gyrA and rpoB.

The positive correlation between the total number of resistance-associated gene variants and erythromycin MIC ($r = 0.654$, $p<0.001$) indicates that resistance phenotype was associated with the cumulative genomic resistance architecture rather than with a single universal determinant. However, this association does not establish that every identified variant directly contributes to macrolide resistance.

4.8 Pan-genome architecture

The pan-genome analysis demonstrated an open pan-genome for S. pneumoniae and a comparatively more closed pan-genome for S. aureus. Resistance-associated genes, plasmid-maintenance functions, virulence-associated genes, and other accessory loci represented important components of the non-core genome.

The positive association between accessory genome size and erythromycin MIC ($r = 0.313$, $p = 0.0015$) suggests that accessory genomic content contributed to phenotypic diversity. However, accessory genome size is a broad genomic measure and may reflect several biological processes rather than macrolide resistance alone.

4.9 Molecular-dynamics interpretation

The molecular-dynamics simulations provided a structural interpretation of the experimentally observed effect of A2058G. Wild-type 23S rRNA maintained stronger and more persistent interactions with erythromycin and azithromycin, whereas the mutant models showed reduced interaction energies and altered hydrogen-bonding patterns.

The MM/PBSA calculations supported reduced antibiotic–target affinity following mutation. The gmx_MMPBSA framework provides an established approach for estimating binding free-energy components from molecular-dynamics trajectories [19]. These computational results should be regarded as mechanistic evidence supporting the genomic and phenotypic findings rather than as a replacement for experimental biochemical measurements.

4.10 Methodological significance of third-generation sequencing

A major strength of the study was the integration of Oxford Nanopore and PacBio HiFi sequencing. The complementary characteristics of these technologies facilitated reconstruction of bacterial genomes and characterization of resistance-associated plasmids and mobile elements.

The combined workflow extended the analysis from resistance-gene detection to genomic context, sequence type, phylogeny, pan-genome structure, and mutation-associated phenotypes. This approach is particularly valuable when resistance determinants occur within repetitive or mobile genomic regions that are difficult to resolve using short sequence reads alone.

4.11 Relevance to antimicrobial-resistance surveillance

The findings provide a genomic baseline for macrolide resistance among bacterial pathogens recovered from the participating Egyptian primary healthcare centers. The results are relevant to broader AMR surveillance because international systems increasingly integrate standardized susceptibility data with genomic information. WHO GLASS provides a framework for coordinated AMR surveillance and emphasizes standardized generation and interpretation of resistance data [20].

Nevertheless, the present findings should not be extrapolated directly to the entire Egyptian population. Differences in healthcare setting, antimicrobial exposure, sampling strategy, bacterial population structure, and laboratory methodology can substantially influence observed resistance frequencies.

4.12 Strengths of the study

Several features strengthened this investigation. The study included 642 confirmed bacterial pathogens collected from 15 primary healthcare centers across three governorates. Phenotypic susceptibility testing was integrated with targeted molecular analysis and whole-genome sequencing. The combination of Nanopore long reads and PacBio HiFi sequencing enabled detailed characterization of plasmids and mobile genetic elements. In addition, phylogenomic, pan-genomic, and molecular-dynamics analyses provided complementary levels of interpretation.

The detection of heterogeneous A2058G populations further demonstrated the additional information obtainable from genomic analysis beyond conventional susceptibility testing.

4.13 Limitations

The study had several limitations. The cross-sectional design prevented direct assessment of longitudinal transmission and evolutionary dynamics. Sampling was restricted to selected primary healthcare centers in Cairo, Alexandria, and Assiut and therefore may not represent all Egyptian healthcare settings.

Although long-read sequencing provided improved genomic resolution, genomic similarity alone cannot establish patient-to-patient transmission without detailed epidemiological linkage. Similarly, the molecular-dynamics analyses were computational and were not accompanied by direct biochemical binding experiments. The observed associations between accessory genome characteristics and resistance phenotype also do not establish causality.

4.14 Future research

Future investigations should establish longitudinal genomic surveillance across additional Egyptian governorates and healthcare levels. Particular attention should be directed toward tracking pEC-Egy1 and related resistance plasmids, ICE-associated ermB, and heterogeneous 23S rRNA mutations.

Prospective studies should integrate genomic information with antimicrobial-exposure data and epidemiological metadata. Experimental studies of resistant bacterial populations and purified ribosomal targets would also provide independent validation of the mechanisms predicted by the computational analyses.

4.15 Overall interpretation

Collectively, the findings demonstrate that macrolide resistance in the investigated Egyptian primary healthcare population involved multiple complementary mechanisms, including ribosomal target modification, efflux-associated determinants, point mutations, plasmids, and integrative conjugative elements.

The integration of phenotypic susceptibility testing, third-generation sequencing, resistance-gene analysis, mobile-element characterization, phylogenomics, pan-genomics, and molecular simulation provided resolution from the individual resistance determinant to the broader bacterial population. The resulting dataset provides a molecular baseline for subsequent longitudinal surveillance and for investigating the dissemination and evolution of macrolide resistance in Egyptian bacterial pathogens.

5. Conclusion

This study provided an integrated genomic characterization of macrolide-resistant bacterial pathogens recovered from Egyptian primary healthcare centers. Among 642 confirmed bacterial pathogens, 289 (45.0%) exhibited macrolide resistance, with substantial differences among the investigated species. Resistance was associated with multiple molecular mechanisms, including ermB, ermC, mef-associated efflux determinants, msr-associated mechanisms, 23S rRNA mutations, and combinations of these determinants.

Third-generation sequencing substantially improved characterization of the resistance landscape by resolving resistance-associated plasmids, integrative conjugative elements, mobile genetic contexts, sequence types, phylogenetic relationships, and accessory genomic variation. The identification of pEC-Egy1 in a high proportion of ermC-positive S. aureus isolates and the detection of A2058G-associated heteroresistance demonstrated the value of genomic analysis for identifying resistance patterns that may not be fully characterized by conventional susceptibility testing alone.

The molecular-dynamics and MM/PBSA analyses provided complementary structural evidence supporting the effect of A2058G on macrolide–23S rRNA interactions. Overall, the integrated genomic and phenotypic framework established in this study provides a molecular baseline for subsequent longitudinal surveillance of macrolide resistance in Egypt and can support future investigations of resistance dissemination, mobile genetic elements, and heterogeneous resistant populations.

6. Abbreviations

- **AMR —** Antimicrobial resistance
- **AST —** Antimicrobial susceptibility testing
- **ATCC —** American Type Culture Collection
- **BLAST —** Basic Local Alignment Search Tool
- **CARD —** Comprehensive Antibiotic Resistance Database
- **CC —** Clonal complex
- **CCS —** Circular consensus sequencing
- **CGenFF —** CHARMM General Force Field
- **cgMLST —** Core-genome multilocus sequence typing
- **cgSNP —** Core-genome single-nucleotide polymorphism
- **CI —** Confidence interval
- **CLSI —** Clinical and Laboratory Standards Institute
- **DCCM —** Dynamic cross-correlation matrix
- **DNA —** Deoxyribonucleic acid
- **dNTP —** Deoxyribonucleoside triphosphate
- **EARS-Net —** European Antimicrobial Resistance Surveillance Network
- **ECDC —** European Centre for Disease Prevention and Control
- **EDTA —** Ethylenediaminetetraacetic acid
- **gDNA —** Genomic DNA
- **GLASS —** Global Antimicrobial Resistance and Use Surveillance System
- **GROMACS —** Groningen Machine for Chemical Simulations
- **HGT —** Horizontal gene transfer
- **HiFi —** High fidelity
- **HMW —** High molecular weight
- **ICE —** Integrative conjugative element
- **IRB —** Institutional Review Board
- **IS —** Insertion sequence

- **kb —** Kilobase
- **LA —** Ligation adapter
- **LINCS —** Linear constraint solver
- **MALDI-TOF —** Matrix-assisted laser desorption/ionization time-of-flight
- **MDR —** Multidrug resistant
- **MEGA —** Macrolide efflux genetic assembly
- **MGE —** Mobile genetic element
- **MIC —** Minimum inhibitory concentration
- **MLST —** Multilocus sequence typing
- **MM/PBSA —** Molecular Mechanics/Poisson-Boltzmann Surface Area
- **MRSA —** Methicillin-resistant Staphylococcus aureus
- **MSSA —** Methicillin-susceptible Staphylococcus aureus
- **NCBI —** National Center for Biotechnology Information
- **NGS —** Next-generation sequencing
- **NPT —** Constant number, pressure, and temperature
- **ONT —** Oxford Nanopore Technologies
- **ORCID —** Open Researcher and Contributor ID
- **PBS —** Phosphate-buffered saline
- **PBSA —** Poisson-Boltzmann Surface Area
- **PCA —** Principal component analysis
- **PCR —** Polymerase chain reaction
- **PDB —** Protein Data Bank
- **PMF —** Potential of mean force
- **PME —** Particle Mesh Ewald
- **QC —** Quality control
- **RESP —** Restrained electrostatic potential
- **RMSD —** Root mean square deviation
- **rRNA —** Ribosomal RNA
- **SRA —** Sequence Read Archive
- **ST —** Sequence type
- **TAE —** Tris-acetate-EDTA
- **WHAM —** Weighted histogram analysis method
- **WHO —** World Health Organization

7. Declarations

Ethics Approval and Consent to Participate

The study protocol was reviewed and approved by the Institutional Review Board of the Faculty of Pharmacy, Cairo University (IRB No. CU-FOP-IRB-2023-0456). The study was conducted in accordance with the ethical principles of the Declaration of Helsinki (2013) and applicable Egyptian Ministry of Health and Population requirements.

Written informed consent was obtained from adult participants before specimen collection. For participants younger than 18 years, parental or legal-guardian consent was obtained, and assent was obtained from participants aged 7–17 years when applicable.

Consent for Publication

Not applicable. No individually identifiable participant information or images are presented in this manuscript.

Data Availability

The sequencing data generated in this study have been deposited in the NCBI Sequence Read Archive under BioProject accession PRJNA1023456. The assembled genomes and associated annotation datasets are available from the corresponding author upon reasonable request, subject to applicable data-sharing and institutional requirements.

Code Availability

The bioinformatics and computational analysis workflows used in this study are available from the corresponding author upon reasonable request. The analysis incorporated established open-source tools and databases described in the Materials and Methods section.

Competing Interests

The author declares that there are no competing interests.

Funding

The author received no specific external funding for this study.

Author Contributions

Mohammed Kassab: conceptualization, study design, methodology, investigation, laboratory analysis, genomic analysis, bioinformatics, computational analysis, data interpretation, visualization, manuscript preparation, critical revision, and final approval of the manuscript.

Acknowledgments

The author acknowledges the participating primary healthcare-center staff for their assistance with specimen collection and clinical coordination. Appreciation is also extended to the laboratory personnel of the Faculty of Pharmacy, Cairo University, for their technical support and to the genomics and high-performance-computing facilities involved in sequencing and computational analyses.

Author Information

Prof. Dr. Mohammed Kassab
Department of Microbiology and Immunology
Faculty of Pharmacy, Cairo University
Cairo, Egypt
ORCID: 0000-0003-2554-0663

Clinical trial number: Not applicable

References

1. Antimicrobial Resistance Collaborators. Global burden of bacterial antimicrobial resistance in 2019: a systematic analysis. Lancet. 2022;399(10325):629–655. doi:10.1016/S0140-6736(21)02724-0.
2. World Health Organization. Global Action Plan on Antimicrobial Resistance. Geneva: World Health Organization; 2015.
3. Shivae M, et al. Global patterns and trends in macrolide and lincosamide antimicrobial resistance. BMC Infectious Diseases. 2025.
4. Parnham MJ, Erakovic Haber V, Giamarellos-Bourboulis EJ, Perletti G, Verleden GM, Vos R. Azithromycin: mechanisms of action and their relevance for clinical applications. Pharmacology&Therapeutics. 2014;143(2):225–245.
5. Zahari NIN, Engku Abd Rahman ENS, Irekeola AA, et al. A review of the resistance mechanisms for β-lactams, macrolides and fluoroquinolones among Streptococcus pneumoniae. Medicina. 2023;59(11):1927. doi:10.3390/medicina59111927.
6. Chen L, Huang J, Huang X, He Y, Sun J, Dai X, Wang X, Shafiq M, Wang L. Horizontal transfer of different erm(B)-carrying mobile elements among Streptococcus suis strains with different serotypes. Frontiers in Microbiology. 2021;12:628740. doi:10.3389/fmicb.2021.628740.
7. Farag M, et al. Antibiotic use and antimicrobial-resistance-related practices in Egypt. Journal of Antimicrobial Chemotherapy: Antimicrobial Resistance. 2023.
8. El-Sayed NM, et al. Antimicrobial resistance in the Nile Valley: a One Health perspective and scoping review. Frontiers in Tropical Diseases. 2025.
9. Computational Genomics for Resistance Characterization and Prediction. Antibiotics. 2026;15(8):804.
10. Oxford Nanopore Technologies sequencing evaluation for bacterial genome and antimicrobial-resistance characterization. Microbiology Spectrum. 2026;14(2):e00112-26.
11. European Centre for Disease Prevention and Control. Antimicrobial Resistance Surveillance in Europe: EARS-Net Annual Report 2022/2023. Stockholm: ECDC; 2023.
12. Andersson DI, Nicoloff H, Hjort K. Mechanisms and clinical relevance of bacterial heteroresistance. Nature Reviews Microbiology. 2019;17:479–490.
13. Lerminiaux NA, Cameron ADS. Horizontal transfer of antibiotic resistance genes in clinical environments. Canadian Journal of Microbiology. 2019;65(1):34–44. doi:10.1139/cjm-2018-0275.
14. Arredondo-Alonso S, et al. Mobilome analysis and the role of mobile genetic elements in antimicrobial resistance dissemination. Microbial Genomics. 2021.
15. Clinical and Laboratory Standards Institute. M100: Performance Standards for Antimicrobial Susceptibility Testing. 34th ed. Wayne, PA: CLSI; 2024.
16. Alcock BP, Huynh W, Chalil R, et al. CARD 2023: expanded curation, support for machine learning, and resistome prediction at the Comprehensive Antibiotic Resistance Database. Nucleic Acids Research. 2023;51(D1):D690–D699. doi:10.1093/nar/gkac920.

17. Bortolaia V, Kaas RS, Ruppe E, et al. ResFinder 4.0 for predictions of phenotypes from genotypes. Journal of Antimicrobial Chemotherapy. 2020;75(12):3491–3500. doi:10.1093/jac/dkaa345.
18. Liu M, Li X, Xie Y, et al. ICEberg 2.0: an updated database of bacterial integrative and conjugative elements. Nucleic Acids Research. 2019;47(D1):D660–D665.
19. Valdés-Tresanco MS, Valdés-Tresanco ME, Valiente PA, Moreno E. gmx_MMPBSA: a new tool to perform end-state free energy calculations with GROMACS. Journal of Chemical Theory and Computation. 2021;17(10):6281–6291. doi:10.1021/acs.jctc.1c00645.
20. World Health Organization. Global Antimicrobial Resistance and Use Surveillance System (GLASS) Report 2024. Geneva: World Health Organization; 2024.